Molecular Cell

Article

The lncRNA *ALPHA* specifically targets chikungunya virus to control infection

Graphical abstract

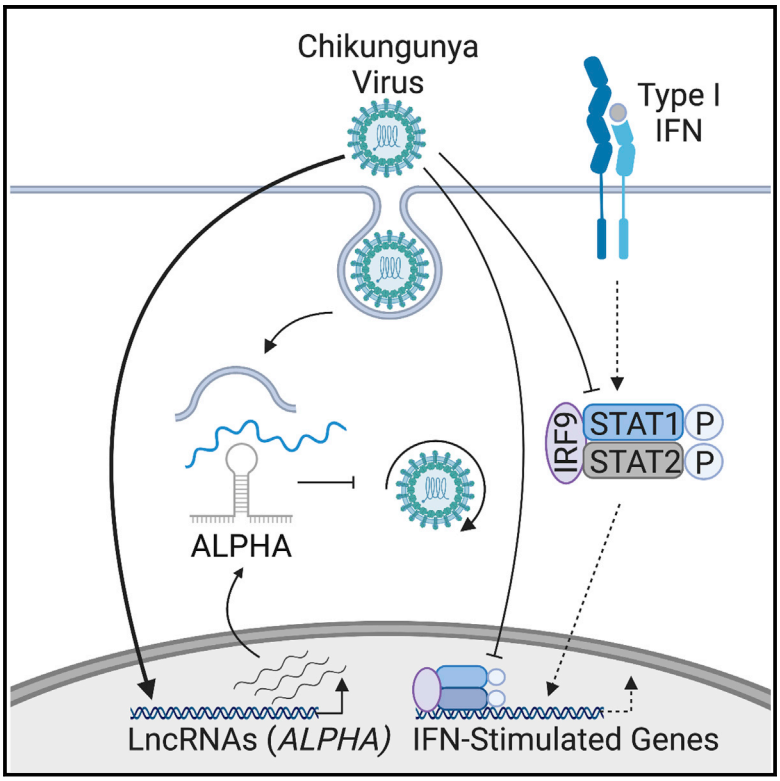

Authors

Megha G. Basavappa, Max Ferretti, Mark Dittmar, ..., Kristen W. Lynch, Jorge Henao-Mejia, Sara Cherry

Correspondence

jhena@pennmedicine.upenn.edu (J.H.-M.), cherrys@pennmedicine.upenn.edu (S.C.)

In brief

Basavappa et al. identify the alphavirus-infection-induced, cytoplasmic, antiviral lncRNA *ALPHA* using high-throughput, loss-of-function screening. *ALPHA* specifically inhibits the replication of the related alphaviruses, chikungunya and O'nyong'nyong virus, but not other alphaviruses. *ALPHA* functions independently of type I IFN signaling, directly binding viral genomic RNA to block viral RNA replication.

Highlights

- High-throughput screening identifies the anti-CHIKV lncRNA *ALPHA*
- *ALPHA* inhibits CHIKV and its closest relative, O'nyong'nyong virus
- *ALPHA* impacts viral RNA replication independently of type I interferon signaling
- *ALPHA* directly binds to CHIKV genomic RNA

Basavappa et al., 2022, Molecular Cell *82*, 3729–3744
October 6, 2022 © 2022 Elsevier Inc.
https://doi.org/10.1016/j.molcel.2022.08.030

CellPress

Molecular Cell

CellPress

Article

The lncRNA *ALPHA* specifically targets chikungunya virus to control infection

Megha G. Basavappa,[1,2] Max Ferretti,[3] Mark Dittmar,[1,2] Julian Stoute,[3] Megan C. Sullivan,[4] Kanupriya Whig,[2,3,5] Hui Shen,[3] Kathy Fange Liu,[3] David C. Schultz,[2,3,5] Daniel P. Beiting,[4] Kristen W. Lynch,[3] Jorge Henao-Mejia,[1,2,6,*] and Sara Cherry[1,2,3,5,7,*]

[1]Department of Pathology and Laboratory Medicine, University of Pennsylvania, Philadelphia, PA 19104, USA
[2]Institute for Immunology, University of Pennsylvania, Philadelphia, PA 19104, USA
[3]Department of Biochemistry and Biophysics, University of Pennsylvania, Philadelphia, PA 19104, USA
[4]Department of Pathobiology, University of Pennsylvania, Philadelphia, PA 19104, USA
[5]High-Throughput Screening Core, University of Pennsylvania, Philadelphia, PA 19104, USA
[6]Division of Protective Immunity, Department of Pathology and Laboratory Medicine, Children's Hospital of Pennsylvania, University of Pennsylvania, Philadelphia, PA 19104, USA
[7]Lead contact
*Correspondence: jhena@pennmedicine.upenn.edu (J.H.-M.), cherrys@pennmedicine.upenn.edu (S.C.)
https://doi.org/10.1016/j.molcel.2022.08.030

SUMMARY

Arthropod-borne viruses, including the alphavirus chikungunya virus (CHIKV), cause acute disease in millions of people and utilize potent mechanisms to antagonize and circumvent innate immune pathways including the type I interferon (IFN) pathway. In response, hosts have evolved antiviral counterdefense strategies that remain incompletely understood. Recent studies have found that long noncoding RNAs (lncRNAs) regulate classical innate immune pathways; how lncRNAs contribute to additional antiviral counterdefenses remains unclear. Using high-throughput genetic screening, we identified a cytoplasmic antiviral lncRNA that we named *antiviral lncRNA prohibiting human alphaviruses* (*ALPHA*), which is transcriptionally induced by alphaviruses and functions independently of IFN to inhibit the replication of CHIKV and its closest relative, O'nyong'nyong virus (ONNV), but not other viruses. Furthermore, we showed that *ALPHA* interacts with CHIKV genomic RNA and restrains viral RNA replication. Together, our findings reveal that *ALPHA* and potentially other lncRNAs can mediate non-canonical antiviral immune responses against specific viruses.

INTRODUCTION

Innate immunity is the first line of defense against all infectious microbes. During viral infection, unusual nucleic acid structures encoded by the virus are ''sensed'' by germline encoded pattern recognition receptor (PRR) families including the retinoic acid inducible gene I (RIG-I)-like receptors (RLRs) and the Toll-like receptors (TLRs) (Chow et al., 2018; Rehwinkel and Gack, 2020a). Engagement of these PRRs leads to the activation of signaling adaptor proteins including mitochondrial antiviral signaling (MAVS) and TIR-domain-containing adapter inducing interferon β (TRIF) (Hou et al., 2011; Seth et al., 2005; Ullah et al., 2016). These adaptors stimulate downstream signaling pathways and *de novo* transcription of diverse innate immune effectors such as the canonical antiviral cytokine family, type I interferons (IFNs). IFN functions in an autocrine and paracrine manner to upregulate hundreds of IFN-stimulated genes (ISGs) that restrict viral infections (Schneider et al., 2014; Schoggins, 2019). In response, many viruses have developed methods to antagonize and evade IFN signaling. These pathways thus lie at the center of an ever-present evolutionary arms race, wherein viruses continually evolve mechanisms to circumvent antiviral immunity, whereas hosts attempt to overcome virus-mediated innate immune antagonism. Since most viruses are ultimately cleared, additional layers of immune regulation and function must exist to counter these viral evasion strategies.

Mosquito-borne viruses represent a diverse subset of medically relevant pathogens with few therapeutic options. Chikungunya virus (CHIKV) reemerged in the early 2000s and has since infected millions of individuals across the globe. CHIKV belongs to the alphavirus family, possesses an ~11.8-kb positive single-stranded (ss)RNA genome, and replicates within the cytoplasm of infected host cells (Solignat et al., 2009). CHIKV displays broad tropism infecting epithelia, endothelia, and a subset of myeloid cells causing disease characterized by debilitating and often chronic arthralgia (Matusali et al., 2019; Schwartz and Albert, 2010). Like many RNA viruses, CHIKV can be sensed by RLR and TLR family members resulting in the induction of type I IFN and ISGs (Fox and Diamond, 2016). However, CHIKV has evolved mechanisms to evade and attenuate these pathways. For example, CHIKV

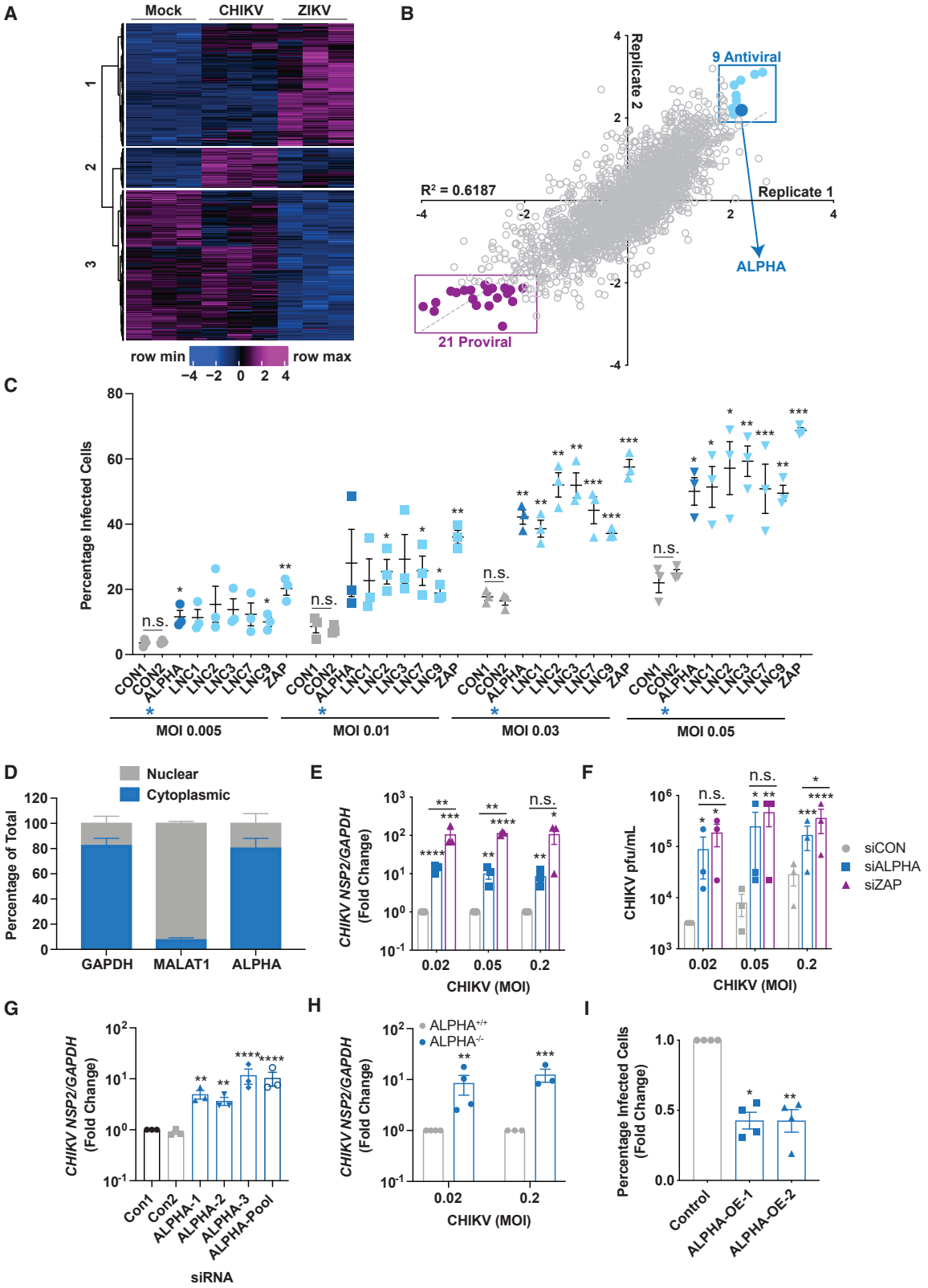

(legend on next page)

non-structural protein (nsp)2 both shuts down global transcription by inhibiting the polymerase (Pol)II cofactor, retinol binding protein (RBP)1, and blocks the phosphorylation of signal transducer and activator (STAT)1 limiting both IFN and ISG production (Akhrymuk et al., 2012, 2019; Fros et al., 2010, 2015; Fros and Pijlman, 2016; Göertz et al., 2018). The full spectrum of host antiviral factors that inhibit CHIKV replication is unknown.

Although many of the protein coding pathways involved in antiviral defense have been characterized, how long noncoding RNAs (lncRNAs) contribute to antiviral immunity is unclear. LncRNAs are defined as any noncoding RNA that is greater than 200 nucleotides in length. These transcripts are Pol II transcribed, 5′ capped, and can be polyadenylated and spliced thus closely mirroring messenger RNAs in terms of their biogenesis except for the definitive lack of an open reading frame (ORF) producing a polypeptide of >100 amino acids (aa). LncRNAs have been shown to regulate various aspects of innate immunity including innate immune cell development, RLR and TLR signaling, and immune gene expression (Agarwal et al., 2020; Agliano et al., 2019; Atianand et al., 2017; Basavappa et al., 2019; Chen et al., 2017; Hadjicharalambous and Lindsay, 2019; Jiang et al., 2018; Kotzin et al., 2016; Lin et al., 2019; Mowel et al., 2018, 2017; Vierbuchen and Fitzgerald, 2021; Wang et al., 2014; Yi et al., 2019). These studies have largely focused on lncRNAs in the context of classical innate immune pathways. Whether lncRNAs play additional roles in the control of RNA viruses and/or counteract immune evasion strategies is not known.

Using RNA sequencing (RNA-seq), we found that lncRNAs are induced by infection in a virus-specific manner. To assess the impact of lncRNAs in anti-CHIKV responses, we performed an unbiased, loss-of-function screen targeting 2,200 human lncRNAs in CHIKV-infected endothelial cells. Using this approach, we identified a subset of lncRNAs with putative antiviral activity against CHIKV including the previously uncharacterized, *antiviral lncRNA prohibiting human alphaviruses* (*ALPHA*). Strikingly, *ALPHA* is induced in response to diverse alphavirus infections but only inhibits a subset of alphaviruses specifically CHIKV and its closest relative, O'nyong'nyong virus (ONNV). Mechanistically, we show that *ALPHA* functions independently of canonical, IFN-dependent responses and instead binds directly to CHIKV genomic RNA to inhibit viral RNA replication. Together, our findings provide evidence that lncRNAs can serve as potent and specific antiviral effectors, adding a new layer to innate antiviral immunity.

RESULTS

CHIKV is a mosquito-borne alphavirus that infects humans and primates and causes symptomatic disease characterized by arthralgia (Burt et al., 2017; Silva and Dermody, 2017). To promote its replication, CHIKV has evolved potent mechanisms to antagonize canonical, type I IFN-dependent signaling (Akhrymuk et al., 2012; 2019; Fros et al., 2010, 2015, 2013, Fros and Pijlman, 2016; Göertz et al., 2018; Meshram et al., 2019). We set out to identify additional mechanisms used by host cells to counteract these CHIKV evasion strategies. We began by exploring the transcriptional response to CHIKV infection. Since endothelial cells are an important target for many viruses including CHIKV, we performed RNA-seq in human brain microvascular endothelial cells (HBMECs) in the presence and absence of CHIKV or the phylogenetically disparate arbovirus, Zika virus (ZIKV). Inclusion of ZIKV allowed us to define pathways commonly induced by viral infection (e.g., IFN) from those that are virus specific. As expected, analysis of differentially induced coding RNAs (mRNAs) revealed significant changes in canonical transcriptional programs including IFNs, ISGs, and NF-κB signaling in both CHIKV and ZIKV-infected cells (Figures S1A and S1B). Notably, both the total number of significantly upregulated transcripts and the relative levels of many induced canonical innate immune genes were reduced in CHIKV-infected cells compared with ZIKV-infected cells (Figures S1A and S1C). This suggests that CHIKV evades canonical signaling to a greater extent than ZIKV as has been previously suggested (Nelemans and Kikkert, 2019). Strikingly, we also found that lncRNAs comprise a substantial portion of the total transcripts induced upon infection and that, unlike classical immune coding genes, the majority of these RNAs are either CHIKV- or

Figure 1. High-throughput, loss-of-function, genome-scale screens reveal antiviral lncRNAs against CHIKV

(A) Heatmap depicting differentially upregulated long noncoding RNAs (lncRNAs) with a $\log_2$-fold change greater than 1, read cutoff of 10, and adjusted p value less than 0.05 in uninfected, CHIKV, or ZIKV-infected HBMEC at 24 h post-infection in three independent experiments. The y axis represents individual annotated lncRNAs.

(B) Results from high-throughput screens targeting 2,200 lncRNAs across the human genome in CHIKV-infected HBMEC. The screen was performed in duplicate, *Z* scores were calculated from percent infection values and replicates were plotted against each other. The 9 anti-CHIKV lncRNAs identified in the screen ($Z > 2$ in both replicates) are highlighted in light blue. *ALPHA* is demarcated by the enlarged, dark blue data point. The 21 proviral lncRNAs are highlighted in purple.

(C) Secondary screens were performed for 6 of the 9 anti-CHIKV candidate lncRNAs using three pooled siRNAs per target followed by infection with CHIKV-mKate for 24 h at the indicated MOIs and the percentage of infected cells was quantified. *ALPHA* is highlighted by dark blue symbols and a blue asterisk.

(D) The relative intracellular localization of *ALPHA* in uninfected HBMEC measured by qPCR and displayed as the percentage of total transcript. *GAPDH* was used a positive control for cytoplasmic enrichment; *MALAT1* was used as a positive control for nuclear enrichment.

(E and F) Control and *ALPHA*-depleted HBMEC were infected with CHIKV for 30 h at the indicated MOIs. Infection levels were quantified by (E) quantitative reverse transcription PCR (qPCR) for viral RNA or (F) $TCID_{50}$s for viral titers.

(G) *ALPHA* was depleted using three independent siRNAs followed by infection with CHIKV at MOI 0.05 for 24 h. Viral RNA was quantified by qPCR.

(H) $ALPHA^{-/-}$ HBMEC were generated using CRISPR-Cas9 and infected with CHIKV for 24 h at the indicated MOIs. CHIKV RNA was measured by qPCR.

(I) HBMEC clones stably expressing *ALPHA* cDNA were infected with MOI 0.2 for 24 h. The percentage of cells infected was quantified by immunofluorescence and automated microscopy. Data are presented as fold change versus control cells in (E) and (G–I). *GAPDH* was used as a loading control gene for all qPCR experiments unless otherwise noted. *$p < 0.05$, **$p < 0.01$, ***$p < 0.001$, ****$p < 0.0001$; error bars represent SEM; screens shown in (B) were performed in duplicate, n = 3–4 for all other experiments as indicated; statistical analyses were performed using Student's (unpaired, two-tailed) t test with Holm-Sidak correction for multiple comparisons (C, E, F, and H), one-way ANOVA with Tukey correction for multiple comparisons (G); one-way ANOVA with Dunnet correction for multiple comparisons (I).

See also Figures S1 and S2.

ZIKV-specific (Figures 1A and S1A–S1C). These data suggest that lncRNAs may serve as key mediators of virus-specific antiviral responses.

To identify lncRNAs with anti-CHIKV activity, we performed a high-throughput RNAi screen targeting 2,200 lncRNAs (designed by Ambion) in HBMEC followed by infection with CHIKV engineered to express an mKate fluorescent reporter during viral replication (CHIKV-mKate, Figures S1D and S1E) (Long et al., 2016; Moser et al., 2016). The screen contained a subset of the lncRNAs identified by RNA-seq. We used automated imaging and imaging analysis to quantify the total number of cells (nuclei counts) and percentage of cells infected (mKate+) (Figure S1D). This screen was performed in duplicate and *Z* scores were calculated for cell number and percent infection (Figures 1B and S1F). As a negative control, we used a scrambled siRNA (siCON); as positive controls for RNAi efficiency, we used siRNAs targeting both pro-mitotic and anti-apoptotic RNAs (si*KIF11* and siDEATH, respectively) (Figure S1G). As a positive control for an antiviral effect, we targeted the canonical immune factor zinc finger antiviral protein (ZAP) (Figure S1H) (Bick et al., 2003; MacDonald et al., 2007). We removed cytotoxic genes ($Z < -2$ for cell number) and plotted *Z* scores calculated from percent infection replicate data (Figures 1B and S1F). Using a cutoff of $Z > 2$, we identified 9 previously uncharacterized, potentially antiviral lncRNAs where RNA depletion resulted in an increase in the percentage of CHIKV-infected cells (Figure 1B). We also identified 21 putative "proviral" lncRNAs using a cutoff of $Z < -2$. It is possible that a subset of these "proviral" lncRNAs represent negative regulators of innate immunity which may be critical to a complete understanding of anti-CHIKV responses. However, we initially focused on the narrower set of 9 antiviral lncRNAs, validating 6 in secondary screens (Figure 1C). In all, these findings identify new lncRNAs with putative activity against CHIKV.

LncRNAs can have nuclear or cytoplasmic activities; nuclear lncRNAs often regulate proximal genes in *cis*, whereas cytoplasmic lncRNAs can have more divergent functions (Basavappa et al., 2019; Mowel et al., 2018). Since CHIKV RNA replication occurs within the cytoplasm of infected cells, we were particularly interested in lncRNAs localized in this compartment. To this end, we isolated nuclear and cytoplasmic fractions from uninfected HBMEC and measured the relative enrichment of lncRNA transcripts in each compartment. We used *GAPDH* (a cytoplasmic mRNA) and *MALAT1* (a nuclear lncRNA) as controls. Using this approach, we found that the Ensembl: *ENST00000452500* transcript is localized in the cytoplasm; we have named this lncRNA *ALPHA* (Figures 1B and 1D). The *ALPHA* locus encodes a human-specific (non-conserved), long intergenic noncoding RNA (lincRNA) located on chromosome 21 (Figure S2A). *ALPHA* exists as a single isoform of 530 bp containing 3 exons (Figure S2A). To verify that *ALPHA* is indeed noncoding, we demonstrated that *ALPHA* is not enriched in polysomes (Figures S2B and S2C). In order to explore *ALPHA* antiviral function more extensively, we assessed how *ALPHA* depletion affects viral protein, RNA, and newly produced virions. We observed significant increases in all three parameters upon *ALPHA* knockdown in HBMEC when compared with control cells, recapitulating the screening results (Figures 1E, 1F, S2D, and S2E). Strikingly, loss of *ALPHA* led to >10-fold increases in both viral RNA and titers, closely mirroring the effects observed by depletion of the anti-alphaviral protein ZAP, indicating that *ALPHA* is a potent inhibitor of CHIKV infection (Figures 1E and 1F). To eliminate the possibility that *ALPHA*'s antiviral effects were a result of RNAi-associated off-target effects, we used three independent siRNAs targeting non-overlapping regions of exons 2 and 3 and measured CHIKV replication. Again, we observed significant increases in viral RNA upon *ALPHA* depletion using each of these siRNAs (Figure 1G). In addition, we generated an HBMEC clone with genetic deletion of the *ALPHA* locus using CRISPR-Cas9. Similar to our RNAi results, we observed significant increases in viral RNA, viral titers, and the percentage of infected cells across different MOIs in $ALPHA^{-/-}$ cells (Figures 1H and S2F–S2H). Finally, we generated HBMEC clones that stably overexpress the single *ALPHA* isoform containing 3 exons and found that CHIKV is significantly attenuated in these cells compared with control infected cells (Figures 1I and S2I). Together, these data indicate that *ALPHA* is a cytoplasmic lncRNA with potent antiviral activity against CHIKV.

To understand *ALPHA* transcriptional regulation during CHIKV infection, we infected HBMEC with CHIKV for 24 h and measured *ALPHA* expression (Figures 2A and S3A). We found that *ALPHA* RNA is potently induced by CHIKV infection in a dose-dependent manner (Figures 2A and S3A). We next assessed whether *ALPHA* is specifically induced by CHIKV or is more broadly upregulated by viral infection. To this end, we infected HBMEC with a set of related alphaviruses including CHIKV, ONNV, Mayaro (MAYV), and Sindbis virus (SINV), or the unrelated arbovirus, ZIKV at MOI 5 for 24 h and quantified *ALPHA* levels (Figure 2B). We found that infection with all alphaviruses tested resulted in a $\geq$10-fold increase in *ALPHA* levels; however, ZIKV infection did not induce *ALPHA* expression (Figure 2B). Thus, *ALPHA* induction may be specific to alphaviral infection. We next addressed whether viral replication is required for this upregulation or whether sensing of incoming particles alone is sufficient. To test this, we infected HBMEC with either wild-type (WT) or UV-inactivated CHIKV (Figure 2C). WT CHIKV infection led to a dose-dependent increase in *ALPHA* expression, whereas UV-inactivated CHIKV did not (Figure 2C). Altogether, these data demonstrate that *ALPHA* is induced in an alphavirus-specific and replication-dependent manner.

Classical cytokines, IFNs, and ISGs are robustly upregulated upon viral infection. As these response mechanisms are not unique to CHIKV (and are induced by ZIKV), it seemed unlikely that these pathways regulated *ALPHA* induction. However, to directly test whether IFN-dependent pathways induce *ALPHA*, we stimulated HBMEC with Sendai virus (SeV), a potent stimulator of RLRs that leads to robust induction of both type I IFN and ISGs, for 24 h and measured *ALPHA* expression (Figures 2D and S3B) (Seth et al., 2005). Notably, although the cells were effectively stimulated as measured by *IFNB1* and *ISG56* transcript levels, *ALPHA* remained unchanged (Figures 2D and S3B). Similarly, direct treatment with recombinant IFNβ for 24 h induced ISGs but did not affect *ALPHA* expression (Figures 2D and S3B). In addition to type I IFN, interleukin (IL)-1β, and tumor necrosis factor (TNF)-α are also important cytokines induced during CHIKV infection (Kelvin et al., 2011; Ng et al., 2009; Tanabe et al., 2018;

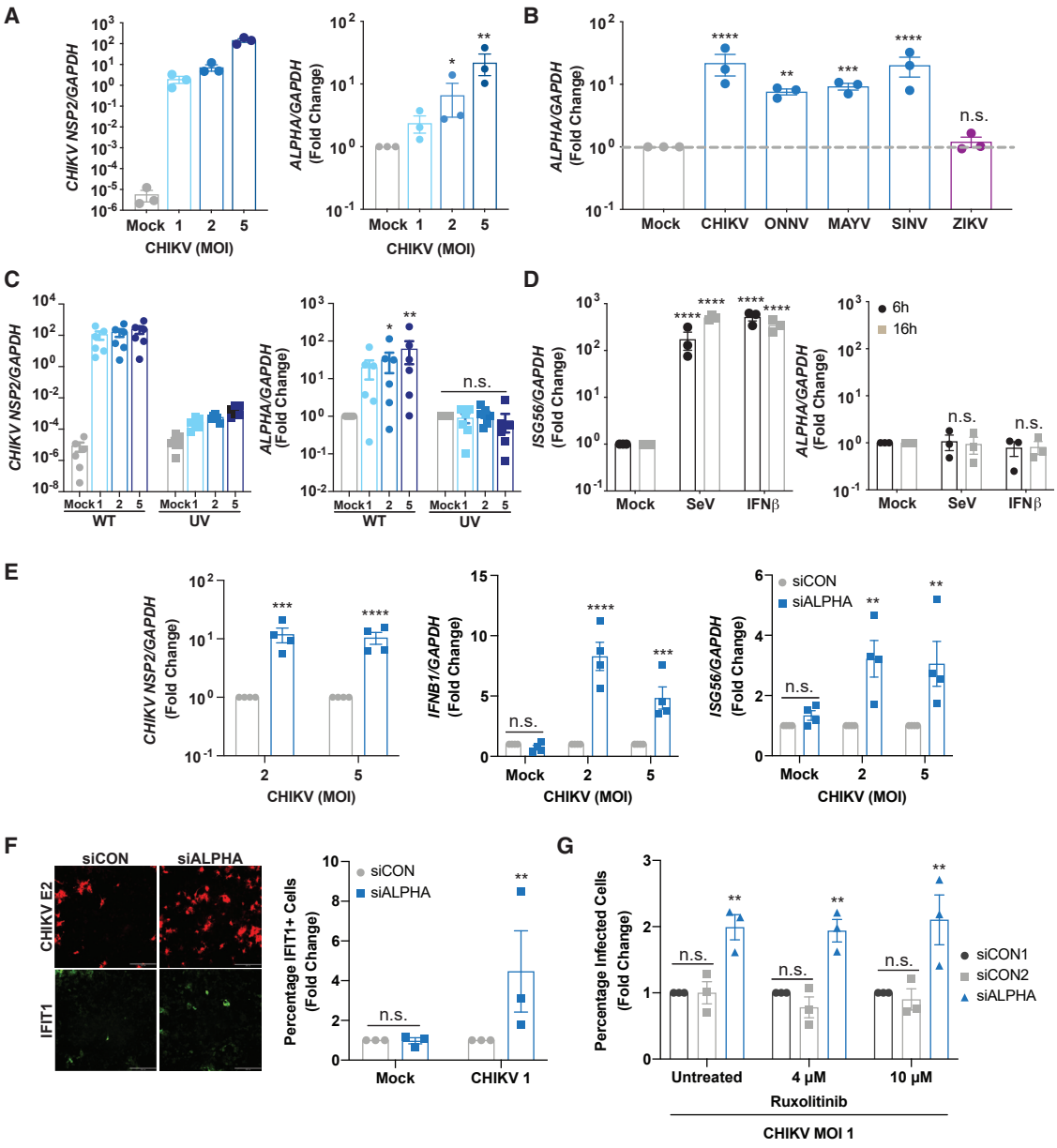

Figure 2. *ALPHA* induction and function is independent of canonical interferon pathways

(A) HBMEC were infected with CHIKV for 24 h at the indicated MOIs. Viral RNA and *ALPHA* levels were quantified by qPCR.

(B) HBMEC were infected with the related alphaviruses CHIKV, O'nyong'nyong (ONNV), Mayaro (MAYV), and Sindbis virus (SINV) or the phylogenetically disparate, ZIKV at MOI 5 for 24 h. *ALPHA* was measured by qPCR.

(C) *ALPHA* transcript levels were measured by qPCR following infection with either wild-type or UV-inactivated CHIKV at the indicated MOIs for 24 h.

(D) HBMEC were stimulated with either Sendai virus (SeV, 100 HAU/mL) or recombinant IFNβ (10 ng/mL) for the indicated time points and *ALPHA* was quantified by qPCR.

(E) Control and *ALPHA*-depleted HBMEC were infected with CHIKV for 24 h at the indicated MOIs. Viral RNA, *IFNB1*, and *ISG56* transcript levels were measured by qPCR.

(F) HBMEC were treated with either control or pooled *ALPHA* siRNAs and infected with CHIKV at MOI 1 for 24 h. IFIT1 protein expression was quantified by immunofluorescence and automated microscopy.

(G) Control and *ALPHA*-depleted HBMEC were pre-treated with ruxolitinib at the indicated concentrations for 2 h. The cells were then spin infected with CHIKV at MOI 1 for 24 h. The percentage of CHIKV-infected cells was measured by immunofluorescence and automated microscopy. Scale bars represent 200 μm. *GAPDH* was used as a loading control in all qPCR experiments. Data are presented as fold change relative to uninfected or unstimulated controls (A–D and F) or siCON (E and G). *p < 0.05, **p < 0.01, ***p < 0.001, ****p < 0.0001; error bars are SEM; n = 3–6 as indicated; statistical analyses were performed using one-way ANOVA with Dunnett correction for multiple comparisons (A), one-way ANOVA with Tukey correction for multiple comparisons (B), two-way ANOVA with Tukey correction for multiple comparisons (C and D), Student's (unpaired, two-tailed) t test with Holm-Sidak correction for multiple corrections (E–G).

See also Figures S3 and S4.

Venugopalan et al., 2014). However, we found that stimulation of HBMEC with either IL-1β or TNF-α for 24 h did not lead to *ALPHA* induction (Figures S3C and S3D). Additionally, we evaluated the contribution of mitogen-activated protein kinase (MAPK) and c-Jun N-terminal kinase (JNK) signaling to *ALPHA* regulation as these cascades have previously been implicated in CHIKV infection (Nayak et al., 2019; Varghese et al., 2016). Although CHIKV infection was modestly decreased upon treatment with the JNK inhibitor SP600125 and the MAPK inhibitor PD98059 as previously described, *ALPHA* induction was not significantly impacted (Figures S3E and S3F) (Nayak et al., 2019; Varghese et al., 2016).

We further mined our own transcriptomics data for CHIKV-induced pathways in HBMEC. One of the most highly induced genes was the prostaglandin $F2_{\alpha}$ ($PGF2_{\alpha}$) receptor (PTGFR, 100-fold). To test whether $PGF2_{\alpha}$ signaling contributes to *ALPHA* induction, we treated HBMEC with a $PGF2_{\alpha}$ antagonist (AL8810), infected cells with CHIKV and measured *ALPHA* levels (Figure S3G). We observed that PTGFR activity was not required for CHIKV-induced *ALPHA* upregulation and did not impact infection (Figure S3G). We also tested the contribution of Ca^{2+} signaling to *ALPHA* regulation as this is a classical signaling pathway used throughout the immune system. To assess whether Ca^{2+} flux impacts *ALPHA* induction, we stimulated HBMEC with the calcium ionophore ionomycin for 24 h and observed no significant difference in *ALPHA* levels (Figure S3H). Together, these data indicate that *ALPHA* induction is specifically induced during alphavirus infection and is independent of classical cytokines, canonical innate immune signaling pathways, and other characterized CHIKV-induced pathways.

We further assessed *ALPHA* induction across other cell types including primary human monocytes, A549 cells (lung epithelial carcinoma cells), and U2OS cells (osteosarcoma cells). CHIKV replicates in these cells as indicated by both CHIKV RNA levels and IFN induction (Figures S3I–S3K). We found that *ALPHA* is neither expressed at baseline nor induced by infection in either monocytes or A549s (Figures S3I and S3J). Interestingly, *ALPHA* is expressed in U2OS at baseline to similar levels as HBMEC but is not induced by CHIKV infection (Figure S3K). These data suggest that *ALPHA* expression is regulated in both a virus- and cell type-specific manner. This supports previous studies demonstrating that lncRNAs typically have more restricted cell expression patterns relative to messenger RNAs (Cabili et al., 2011; Hon et al., 2017; Werner et al., 2017).

We next set out to define the mechanism by which *ALPHA* attenuates CHIKV infection. Although we found that *ALPHA* induction is independent of IFN, we wanted to assess whether *ALPHA* inhibits infection by regulating IFN-dependent signaling as has been shown for other lncRNAs. (Agarwal et al., 2020; Atianand et al., 2017; Basavappa et al., 2019; Chen et al., 2017; Mowel et al., 2018; Vierbuchen and Fitzgerald, 2021). To this end, we compared *IFNB1* and *ISG56* transcript levels in control and *ALPHA*-depleted cells infected with CHIKV (Figure 2E). If *ALPHA* promotes this pathway, we would have expected decreased levels of *IFNB1* and *ISG56* upon loss of *ALPHA*. In contrast, we observed elevated levels of these transcripts compared with control cells likely as a consequence of the increased viral infection that occurs upon *ALPHA* depletion (Figure 2E). We further explored the impact of *ALPHA* on IFN by generating a HBMEC line which stably expresses an IFN-mCherry reporter. Using this tool, we assessed the contribution of *ALPHA* to IFN regulation outside of CHIKV infection. As expected, at baseline, there was no detectable IFN-mCherry expression; however, upon infection with SeV, reporter expression was robustly induced in a dose-dependent manner (Figures S4A and S4B). We depleted *ALPHA* in these cells followed by infection with SeV for 24 h and quantified reporter signal by automated microscopy. As a positive control, we included siRNAs targeting MAVS, a canonical adaptor protein required for IFN induction downstream of SeV infection (Seth et al., 2005). As expected, MAVS depletion caused a significant loss in both the percentage of IFN-mCherry+ cells as well as total mCherry protein as measured by mean fluorescent intensity (MFI, Figures S4A and S4B). In contrast, we observed no difference in IFN-mCherry expression in *ALPHA*-depleted cells compared with control (Figures S4A and S4B). Given that cytoplasmic lncRNAs can also modulate protein translation in diverse biological contexts, we also tested whether *ALPHA* regulates ISG translation (Basavappa et al., 2019; Mowel et al., 2018). To test this, we depleted *ALPHA* in HBMEC, infected with CHIKV for 24 h, and quantified IFIT1 protein levels by immunofluorescence and automated microscopy (Figure 2F). Again, we found that *ALPHA* is not required for ISG protein production. Instead, we observed that IFIT1 protein levels were increased upon *ALPHA* knockdown (Figure 2F). Together, these data suggest that *ALPHA* antiviral function is independent of IFN and ISG transcription or translation.

To address whether *ALPHA* antiviral activity is dependent on IFN signaling, we infected control or *ALPHA*-depleted HBMEC with CHIKV in the presence of the janus kinase (JAK)1/2 inhibitor, ruxolitinib, which potently inhibits ISG induction (Figures 2G and S4C) (Chiappinelli et al., 2015; Stewart et al., 2014). As expected, ruxolitinib treatment led to a marked attenuation in CHIKV-induced IFIT1 production (Figure S4C). Moreover, we observed that in *ALPHA*-depleted cells, the percentage of infected cells was significantly elevated compared with control cells in both untreated and ruxolitinib-treated cells (Figure 2G). These findings together indicate that *ALPHA* anti-CHIKV activity is independent of IFN signaling.

A hallmark of type I IFN is its broad potency against diverse viral families. However, we found that *ALPHA* is specifically induced by alphaviruses and has anti-CHIKV activity independent of classical IFN signaling. This led us to hypothesize that *ALPHA* may instead have restricted antiviral activity against alphaviruses. To test this possibility, we depleted *ALPHA* in HBMEC and infected with diverse alphaviruses including CHIKV, ONNV, SINV, MAYV, and Ross River virus (RRV, phylogeny shown in Figure 3A). In addition to increasing CHIKV infection, *ALPHA* depletion resulted in a significant increase in ONNV-infected cells, viral RNA, and titers (Figures 3B and 3C). Strikingly, however, there was no effect on more distant alphaviruses including MAYV, SINV, and RRV (Figure 3D). In addition, we also tested *ALPHA*'s antiviral activity against other unrelated viruses including ZIKV, influenza A (IAV), Rift Valley fever (RVFV), La Crosse (LACV), and herpes simplex I (HSV-1) and found that loss of *ALPHA* had no effect on the replication of any these viruses (Figures 3E and S4D–S4G). In contrast, knockdown of the broadly acting anti-alphaviral factor ZAP, resulted in an

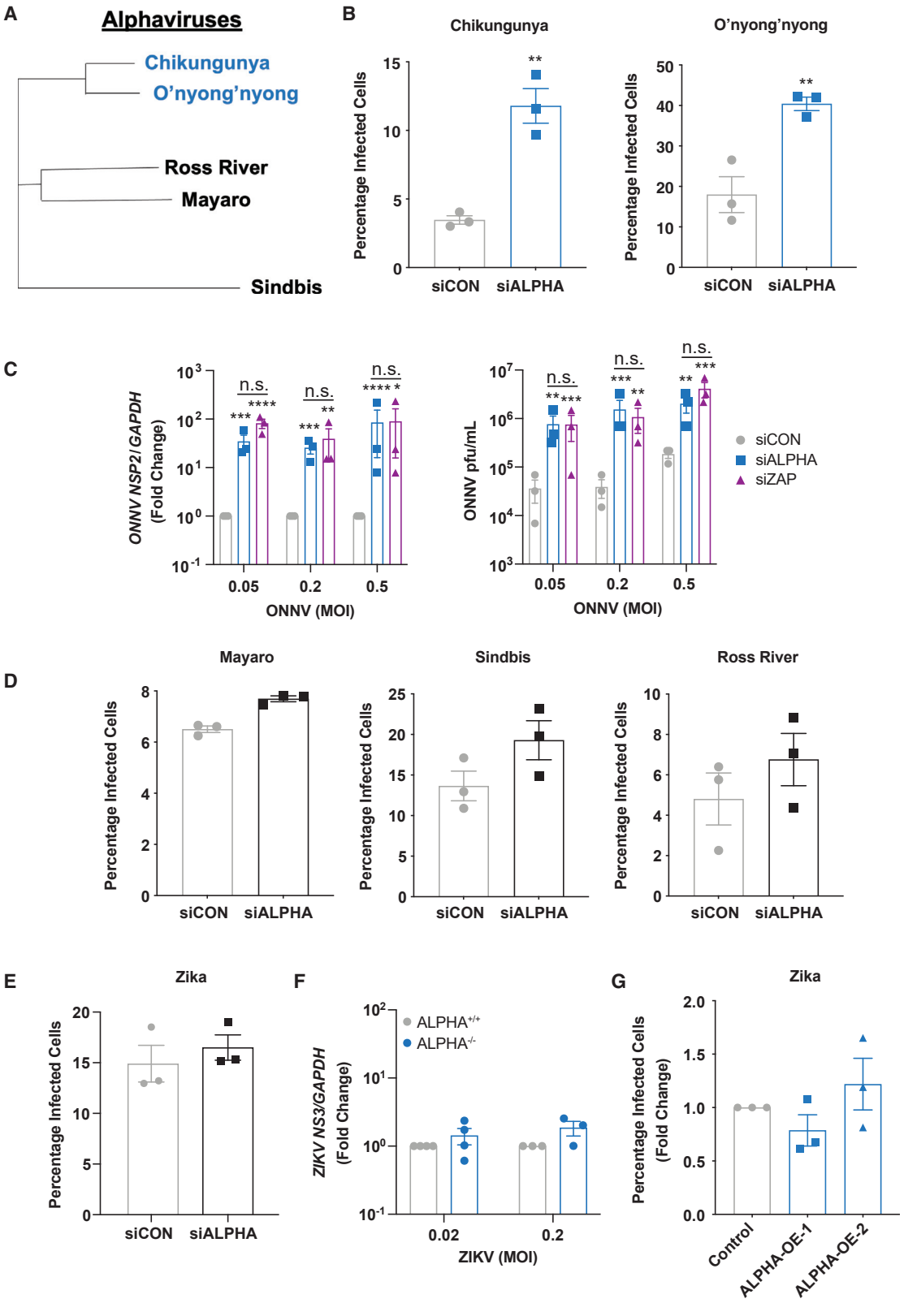

(legend on next page)

increase in infection across multiple alphaviruses (Figure S4H). Furthermore, we infected both *ALPHA*$^{-/-}$ *and ALPHA*-overexpressing HBMEC with ZIKV and observed no change in infection in either cell population compared with controls (Figures 3F and 3G). Altogether, these results demonstrate that the antiviral activity of *ALPHA* is highly restricted to the closely related alphaviruses CHIKV and ONNV.

We next explored how *ALPHA* interferes with the CHIKV replication cycle. Briefly, after binding to its cognate receptor on the plasma membrane, CHIKV is internalized into the endocytic compartment and fuses to the endosome upon acidification, releasing its genome into the cytoplasm. The 5′ ORF is translated by host ribosomes to produce the nsp1–4 polyprotein that is cleaved to form the replicase complex. The replicase then synthesizes anti-genome templates, new genome copies and subgenomic RNAs (encoding the 3′ ORF translated into the structural proteins). New virions are assembled, exit the cell at the plasma membrane, and infect additional cells leading to secondary infection and viral spread. To first test viral entry, we infected HBMEC in the presence of cycloheximide (CHX) that inhibits viral translation, the first step in intracellular viral replication. Measuring internalized viral RNA in this context thus allows for the specific quantification of only viral genomes that have entered into the cells. Using this approach, we observed equivalent levels of viral genomic RNA in control and *ALPHA*-depleted cells indicating that *ALPHA* does not regulate early entry (Figure S5A). We also assessed viral spread by treating cells with ammonium chloride (NH_4Cl) after virus entry. This inhibits endocytic acidification required for secondary infection. As expected, blocking spread reduced overall viral levels in both control and *ALPHA*-depleted HBMEC (Figure S5B). However, viral RNA levels remained significantly increased upon *ALPHA* depletion even in the presence of NH_4Cl, demonstrating that *ALPHA* does not affect viral spread (Figure S5B). Together, these data indicate that *ALPHA* activity modulates an intracellular step of the CHIKV life cycle.

A crucial step in the cytoplasmic CHIKV life cycle is the generation of genome and anti-genome copies. These transcripts form double-stranded (ds)RNA intermediates that can be detected using a specific antibody (J2). We depleted *ALPHA* in HBMEC followed by infection with CHIKV at MOI 20 for 8 h, immunostained with J2, and quantified dsRNA puncta by confocal microscopy. Using this approach, we observed a significant increase in dsRNA puncta in *ALPHA* knockdown conditions compared with control cells (Figures 4A and S5C). Interestingly, a bifurcation in the dsRNA+ population appears specifically in *ALPHA*-depleted cells. This may reflect the non-synchronized manner of infection wherein different cells become infected at different times and those that express higher levels of *ALPHA* are more restrictive in control cells. Overall, these data suggest that *ALPHA* attenuates early viral RNA replication.

We next assessed which specific step of viral RNA replication is impacted by *ALPHA*. The first step in the production of new viral genomes is the generation of anti-genome RNA. An impact on this initial step would consequently alter the downstream levels of both genomic and subgenomic RNAs as well as viral titers. We quantified the number of CHIKV anti-genome copies present in control and *ALPHA*-depleted HBMEC using strand-specific RT-qPCR. We found a significant increase in anti-genome copies upon *ALPHA* knockdown compared with control (Figure 4B). These data show that *ALPHA* affects early viral replication by inhibiting anti-genome production.

Given the observed decrease in CHIKV RNA replication as well as the specificity of *ALPHA* antiviral function, we hypothesized that *ALPHA* may directly bind to CHIKV genomic RNA. Indeed, analysis of the alphaviruses used in this study revealed that the nucleotide sequences between alphaviral genomes are more divergent than the aa sequences they encode (Figure S5D). ONNV is closest to CHIKV at both the nucleotide and protein levels (Figure S5D). We thus hypothesized that *ALPHA* may bind directly to CHIKV genomic RNA to mediate its antiviral effect. To test this hypothesis, we adapted a previously described proximity ligation assay (PLA) to visualize *ALPHA*-CHIKV RNA interactions *in situ* (Figure 4C) (Fredriksson et al., 2002; Söderberg et al., 2006; Zhang et al., 2016). We designed tripartite, antisense, DNA probes containing (1) a 35–45 mer complementary to either *GAPDH*, *ALPHA*, or CHIKV RNA, (2) a poly(A) linker, and (3) a non-specific PLA oligonucleotide overhang. We paired the CHIKV probe with either the *GAPDH* probe as a negative control (CHIKV + GAPDH), a second CHIKV probe 50 bp downstream of the original probe as a positive control (CHIKV + CHIKV), or the *ALPHA* probe (CHIKV + ALPHA). As an additional negative control, we also paired the *GAPDH* probe with an *ALPHA* probe (GAPDH + ALPHA). We allowed these partnered probes to hybridize with RNAs within fixed, permeabilized, CHIKV-infected HBMEC. This was followed by incubation with T4 ligase and PLA "connector" oligos complementary to the probe PLA overhangs. If the two partner probes are in close

Figure 3. *ALPHA* antiviral activity is restricted to CHIKV and ONNV

(A) Phylogenetic tree of the indicated alphaviruses generated using whole genome nucleotide sequences (in VIPR).

(B and D) Control and *ALPHA*-depleted HBMEC were infected for 24 h with CHIKV-mKate (MOI 0.03), ONNV (MOI 0.1), MAYV (MOI 0.1), SINV-mKate (MOI 0.1), and Ross River-GFP (RRV-GFP, MOI 0.3). The percentage of cells infected was measured by immunofluorescence and automated microscopy.

(C) Viral RNA measured by qPCR and viral titers measured by $TCID_{50}$ in control and *ALPHA*-depleted HBMEC infected with ONNV at the indicated MOIs for 30 h. Viral RNA data are displayed as fold change versus control cells.

(E) Control and *ALPHA*-depleted HBMEC were infected with ZIKV (MOI 0.03) for 24 h. Percent infection was measured using immunofluorescence and automated microscopy.

(F) *ALPHA*$^{+/+}$ and *ALPHA*$^{-/-}$ HBMEC were infected with ZIKV at the indicated MOIs for 24 h. Viral RNA was quantified by qPCR.

(G) *ALPHA*-overexpressing cells were infected with ZIKV MOI 0.1 for 24 h. The percentage of cells infected was quantified by immunofluorescence and automated microscopy. Data are displayed as fold change relative to control. $^{**}p < 0.01$, $^{***}p < 0.001$, $^{****}p < 0.0001$; error bars are SEM; n = 3; statistical analyses were performed using Student's (unpaired, two-tailed) t test (B, D, and E), Student's (unpaired, two-tailed) t test with Holm-Sidak correction for multiple comparisons (C and F), one-way ANOVA with Dunnett correction for multiple comparisons (G).

See also Figure S4.

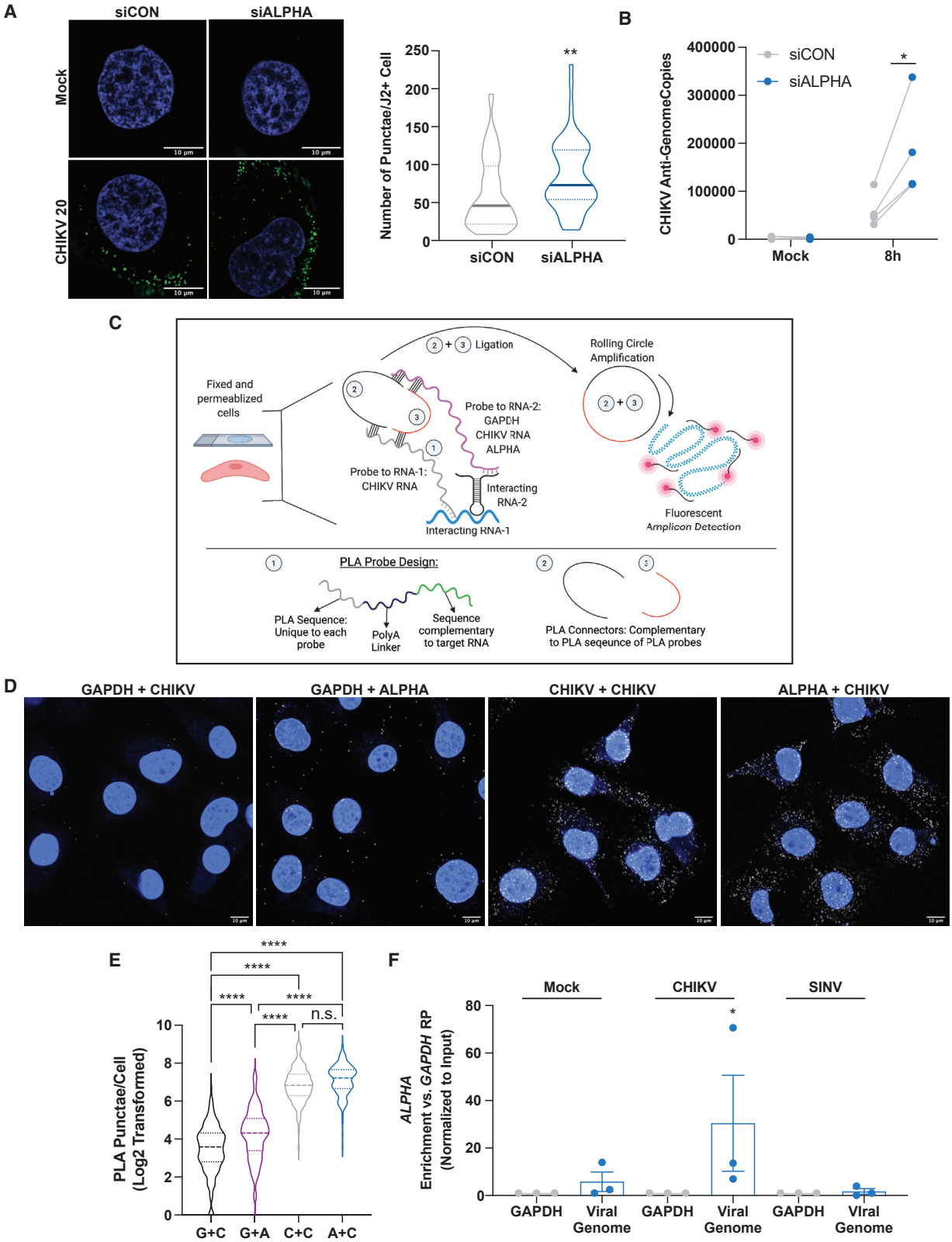

(legend on next page)

proximity, the connector oligos will be ligated to form a circle that serves as a template for rolling circle amplification. The PCR product can then be detected using a fluorescently conjugated antisense DNA probe specific to the amplicon. As expected, we observed very few PLA puncta in GAPDH + CHIKV and GAPDH + ALPHA samples and many puncta in CHIKV + CHIKV samples (Figures 4D, 4E, and S5E). Interestingly, we also found a high number of PLA puncta in ALPHA + CHIKV samples that was significantly greater than that observed in either negative control (Figures 4D, 4E, and S5E). These results suggest that *ALPHA* interacts with CHIKV genomic RNA. These data also reveal that this interaction occurs in the cytoplasm as is expected given that both *ALPHA* RNA and CHIKV RNA replication are localized in this compartment.

To assess RNA-RNA interactions more directly, we used a modified chromatin isolation by RNA pull-down (ChIRP) approach (Figure S6A) (Chu et al., 2012). Briefly, we used glutaraldehyde to crosslink uninfected, CHIKV-, or SINV-infected *ALPHA*-overexpressing HBMEC. In addition to serving as a control for *ALPHA*'s binding specificity, inclusion of SINV-infected cells also provides an important control for *ALPHA* transcript levels as SINV induces *ALPHA* to similar levels as CHIKV but is not sensitive to *ALPHA* antiviral activity (Figures 2B and 3D). Lysates were generated and incubated with 500 nt biotinylated, antisense oligonucleotide (ASO) probes designed against target RNAs of interest specifically *GAPDH* (as a negative control), CHIKV genomic RNA, and SINV genomic RNA. Following hybridization, the biotinylated probes were enriched using streptavidin and relative RNA levels of both the target RNAs and any co-precipitated RNAs were quantified. Using this assay, we effectively enriched for viral genomes using viral probes compared with the control *GAPDH* probe (Figures S6B and S6C). Conversely, the control *GAPDH* probe successfully enriched for *GAPDH* compared with either viral probe (Figure S6D). Importantly, the relative levels of *GAPDH* enrichment were similar across conditions indicating a lack of bias between samples (Figure S6D). We further quantified *ALPHA* levels in both control *GAPDH* and viral RNA pull-downs. As *ALPHA* was not directly targeted by a probe, any positive *ALPHA* signal detected in this assay is a result of co-precipitation and reveals interactions with target RNAs. Strikingly, we observed a significant and specific enrichment in *ALPHA* upon CHIKV RNA pull-down but not SINV RNA pull-down (Figure 4F). Importantly, *ALPHA* enrichment was absent in uninfected cells incubated with the CHIKV genomic RNA probe, demonstrating a requirement for CHIKV RNA (Figure 4F). We repeated these experiments in WT HBMEC and observed a similar, specific enrichment of endogenous *ALPHA* only upon CHIKV RNA pull-down (Figures S6E–S6H).

We next explored whether the *ALPHA*-CHIKV RNA interaction can form independently of other cellular factors. We used purified RNAs to quantify the interaction between *ALPHA* and CHIKV RNA *in vitro*. We *in vitro* transcribed and biotinylated full-length *ALPHA* as well as a truncated *GAPDH* RNA of equivalent length, as a negative control (500 nt, Figures 5A, S6I, and S6J). As a positive control, we also generated a biotinylated, antisense probe complementary to the nsp3 region of the CHIKV genome and of similar length to *ALPHA* (500 nt, Figures 5A, S6I, and S6J). We incubated each of these RNAs with unbiotinylated CHIKV replicon RNA which contains the 5′ end of the CHIKV genome encoding nsp1–4 (7.5 kb) (Jones et al., 2017). We then enriched for each biotinylated RNA (*GAPDH*, nsp3, or *ALPHA*) using streptavidin-conjugated beads and quantified the amount of co-precipitated CHIKV replicon RNA (Figure 5A). We observed significant enrichment of the CHIKV replicon with the positive control compared with *GAPDH* confirming specificity (Figure 5B). Interestingly, we also found that replicon RNA is highly enriched upon pull-down of full-length *ALPHA* (Figure 5B). Importantly, these results further demonstrate that the *ALPHA*-CHIKV RNA interaction does not require protein and pinpoints the interaction within the 5′ end of the CHIKV genome.

We utilized this *in vitro* RNA interaction system to begin mapping the sequence requirements within *ALPHA* to bind CHIKV RNA. We first generated ~250-nt truncations in *ALPHA* spanning exons 1 and 2 (Ex1/2), exon 3 alone (Ex3), and exon 2 and half of exon 3 (Ex2/3, encoding the middle 250 nt of the *ALPHA* transcript). These RNAs were biotinylated and subsequently used as probes to assess *in vitro* interaction with unbiotinylated CHIKV replicon RNA. We observed that exons 1 and 2 are

Figure 4. *ALPHA* binds CHIKV genomes in the cytoplasm to inhibit viral RNA replication

(A) Control and *ALPHA*-depleted HBMEC were infected with CHIKV at MOI 20 for 8 h and dsRNA/J2+ puncta were detected by immunofluorescence and confocal microscopy. The number of puncta per infected cell was quantified by ImageJ in >50 cells per experiment in three independent experiments. Scale bars represent 10 μm.

(B) Anti-genome copies were quantified using strand-specific RT-qPCR in control and *ALPHA*-depleted HBMEC infected with CHIKV at MOI 0.5 for 8 h.

(C) Schematic detailing RNA-PLA. Fixed, permeabilized CHIKV-infected HBMEC were incubated with paired, DNA probes containing a 35–45 nt antisense sequence complementary to target RNAs of interest (i.e., *GAPDH*, CHIKV, and *ALPHA*), a polyA linker, and a unique PLA oligo sequence. Two PLA connector oligos which can bind the PLA probes are introduced into the cells along with T4 ligase. If the PLA probes are near each other (indicating that the target RNAs are in close proximity), the PLA connectors will be ligated into a circle which can then serve as a template for rolling circle amplification (RCA). The resulting amplicon can then be detected using a Cy5-conjugated antisense DNA probe and confocal microscopy.

(D and E) HBMEC were infected with CHIKV at MOI 5 for 24 h and hybridized with PLA probe pairs GAPDH + CHIKV (G + C), GAPDH + ALPHA (G + A), CHIKV + CHIKV (C + C), or ALPHA + CHIKV (A + C). PLA amplicons were visualized as described above. Scale bars represent 10 μm.

(E) PLA puncta per cell were quantified for 3 independent experiments in 40–60 cells per experiment using ImageJ.

(F) *ALPHA*-overexpressing HBMEC were either uninfected or infected with CHIKV or SINV at MOI 2 for 20 h and subjected to glutaraldehyde crosslinking, overnight antisense probe hybridization, streptavidin pull-down, and quantification of both target RNAs (*GAPDH*, CHIKV genomic RNA, or SINV genomic RNA) as well as co-precipitated RNAs (*ALPHA*) by qPCR. Displayed is the relative enrichment of *ALPHA* in each conditions. All data were first normalized to input levels of each transcript and displayed as fold change relative to *GAPDH* pull-down levels (*GAPDH* RP). *$p < 0.05$, **$p < 0.01$, ****$p < 0.0001$; error bars represent SEM; n = 3 (A, C, and D), n = 4 (B); statistical analyses were performed using Student's (unpaired, two-tailed) t test (A), two-way ANOVA with Sidak correction for multiple comparisons (B), one-way ANOVA with Tukey correction for multiple comparisons (D), one-way ANOVA with Sidak correction for multiple comparisons.

See also Figures S5 and S6.

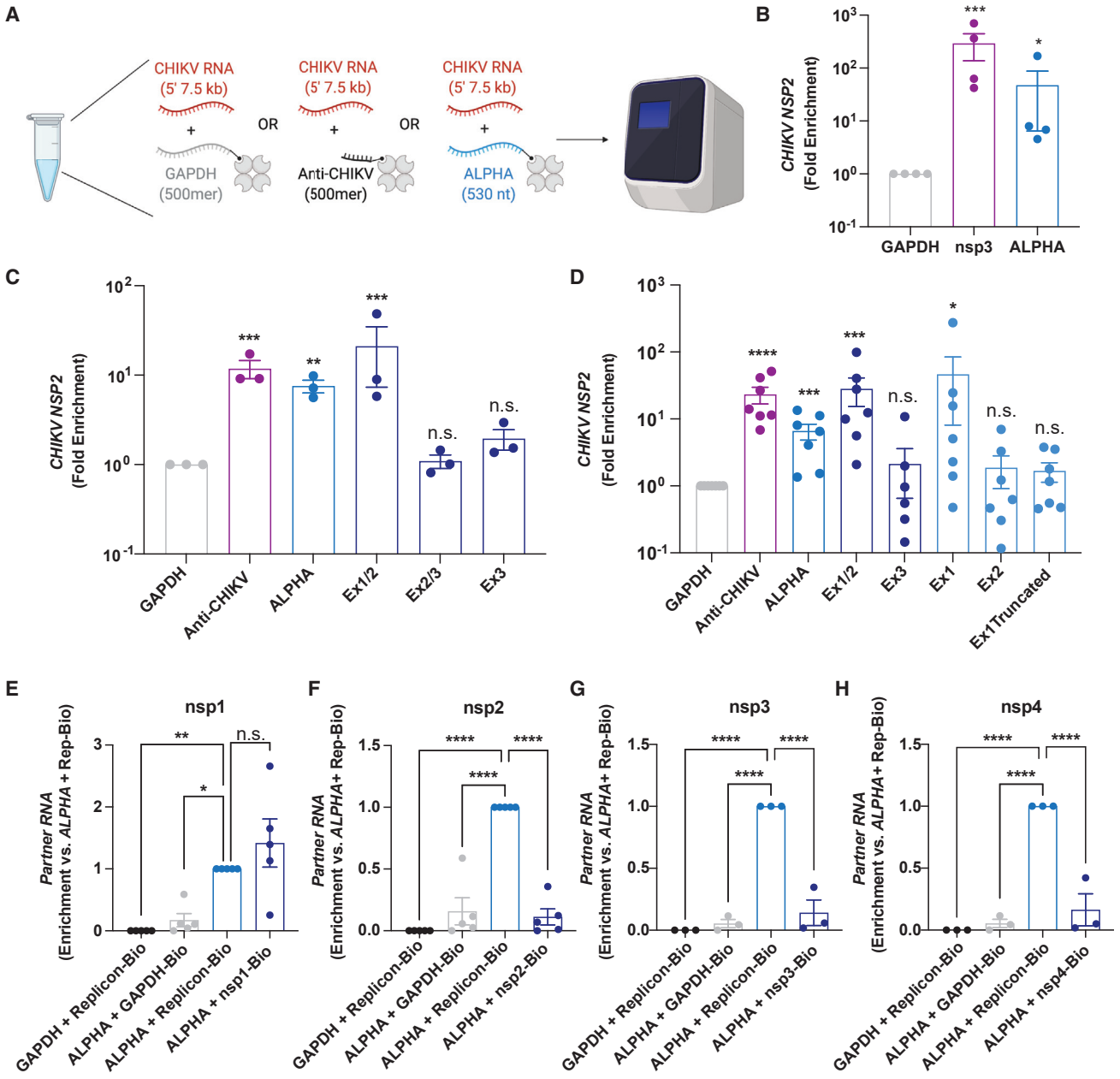

Figure 5. *ALPHA* exon 1 and CHIKV nsp1 interact

(A and B) *In vitro* transcribed, biotinylated *GAPDH*, antisense CHIKV probe (anti-CHIKV), or full-length *ALPHA* were incubated with CHIKV replicon RNA and enriched using streptavidin-conjugated beads. The relative levels of co-precipitated replicon RNA were quantified by qPCR.

(C) *In vitro* transcribed RNAs spanning *ALPHA* exon 1/2 (Ex1/2), exon 3 (Ex3), and exon 2/part of exon 3 (Ex2/3) were biotinylated and used as in (A).

(D) *In vitro* transcribed RNAs spanning *ALPHA* exon 1 alone (Ex1), exon 2 alone (Ex2), and exon 1 with a deletion of the last 12 nt (Ex1Truncated) were biotinylated and used as in (A).

(E–H) Individual nsps1–4 were *in vitro* transcribed, biotinylated, and mixed with either truncated *GAPDH* or *ALPHA*. The relative levels of unbiotinylated *GAPDH* or *ALPHA* was measured by qPCR. Data are presented as fold enrichment versus *GAPDH* (B–D) or ALPHA + full-length CHIKV replicon RNA (E–H). *p < 0.05, **p < 0.01, ***p < 0.001, ****p < 0.0001; error bars represent SEM; n = 3–7 as indicated; Statistical analyses were performed using one-way ANOVA with Dunnett correction for multiple comparisons (B, C, and E–H) or multiple, unpaired, two-tailed Student's t tests (D).

See also Figures S6 and S7.

essential for binding to CHIKV RNA, whereas exon 3 is dispensable (Figures 5C, S6I, and S6J). Next, we made smaller truncations in exons 1 and 2 that were again assessed for binding to CHIKV RNA. These probes include exon 1 only (Ex1), exon 2 only (Ex2), and a truncated Ex1 missing the last 12 nt (Ex1Truncated). We found that exon 1 is required for interaction

with CHIKV RNA (Figures 5D, S6I, and S6J). Interestingly, deletion of the last 12 nt of exon 1 results in loss of CHIKV RNA enrichment closely mirroring levels seen for the *GAPDH* negative control (Figures 5D, S6I, and S6J). These results indicate that the 3′ end of *ALPHA* exon 1 is minimally required for binding to the CHIKV genome.

We also used this *in vitro* RNA interaction system to identify regions within the CHIKV replicon RNA that are bound by *ALPHA*. The CHIKV genome is 11.8 kb in length; the replicon RNA we used in our initial interaction mapping experiments contains the first 7.5 kb, encoding nsp1–4. We generated biotinylated RNAs encoding each nsp and tested their interactions with unbiotinylated, full-length *ALPHA*. As negative controls, we paired unbiotinylated *GAPDH* with full-length biotinylated CHIKV replicon RNA or we paired unbiotinylated *ALPHA* with biotinylated *GAPDH* (Figures 5E–5H, S6K, and S6L). As a positive control, we paired unbiotinylated *ALPHA* with biotinylated full-length CHIKV replicon RNA, paralleling the control conditions from our previous *in vitro* experiments but with the opposite RNA biotinylated (Figures 5E–5H, S6K, and S6L). As above, we incubated partnered RNAs together to form interactions, enriched for biotinylated RNAs using streptavidin-conjugated beads, and quantified the relative levels of the unbiotinylated RNA partners, *GAPDH* or *ALPHA*. As anticipated based on our previous results, *ALPHA* was significantly enriched by full-length biotinylated replicon RNA relative to *GAPDH* in all experiments (Figures 5E–5H, S6K, and S6L). Similarly, *ALPHA* was not bound to biotinylated *GAPDH*, paralleling our findings by RNA-PLA (Figures 4C, 4D, 5E, 5H, S6K, and S6L). When we assessed the individual nsps, we found a striking enrichment in *ALPHA* upon pull-down with nsp1, similar to the levels observed for full-length replicon (Figures 5E, S6K, and S6L). Notably, *ALPHA* did not interact with nsp2, nsp3, or nsp4, closely mirroring our negative controls (Figures 5F–5H, S6K, and S6L). These results thus indicate that *ALPHA* interacts within nsp1 of the CHIKV genome.

Together, these data identify *ALPHA* as a new antiviral lncRNA required for cytoplasmic recognition and control of CHIKV infection and suggests a larger role for lncRNAs as antiviral effectors capable of directly inhibiting viral infection independently of canonical IFN signaling (Figure S7A).

DISCUSSION

Innate antiviral immune pathways lie at the center of a constant evolutionary arms race between host and virus. To survive infection, hosts use diverse mechanisms to overcome virus-mediated immune evasion. (Ma and Suthar, 2015; Nelemans and Kikkert, 2019). LncRNAs have recently been shown to be critical regulators of canonical innate immune responses including type I IFN signaling (Agliano et al., 2019; Atianand et al., 2017; Basavappa et al., 2019; Carpenter and Fitzgerald, 2018; Chen et al., 2017; Hadjicharalambous and Lindsay, 2019; Mowel et al., 2018; Rehwinkel and Gack, 2020a; Yi et al., 2019). Here, we identified a set of both putative antiviral and proviral lncRNAs including *ALPHA* that functions as an anti-CHIKV effector independently of canonical IFN signaling. Indeed, we found that *ALPHA* specifically inhibits CHIKV and its closest relative ONNV but not other viruses tested. Thus, our findings demonstrate that lncRNAs can selectively target specific subsets of viruses outside of IFN-mediated pathways. Whether the other 5 validated antiviral lncRNAs identified in this study function in a similar way to *ALPHA* will be essential in understanding whether antiviral specificity and IFN-independence are a broader hallmark of antiviral lncRNAs. Further investigation of the proviral lncRNAs identified in this study may also reveal new mechanisms by which lncRNAs can facilitate viral infection and/or serve as negative regulators of innate immunity, potentially adding another layer to our understanding of innate immune signaling.

Our transcriptomics revealed that hundreds of lncRNAs are induced upon infection in a virus-specific manner. Furthermore, we found that *ALPHA* is highly induced upon infection with alphaviruses but not the unrelated arbovirus ZIKV. This suggests that viral specificity may be a shared characteristic of non-canonical, antiviral lncRNA transcriptional regulation. Further exploration into the signal that drives *ALPHA* induction showed that unlike other innate lncRNAs, broadly acting immune pathways including IFN are dispensable for *ALPHA* transcriptional induction (Atianand et al., 2017; Basavappa et al., 2019; Elling et al., 2016; Mowel et al., 2018; Vierbuchen and Fitzgerald, 2021). These data therefore suggest that *ALPHA* expression is controlled by an unknown alphavirus-specific pathway. This is particularly provocative as alphavirus-encoded nsp2 localizes to the nucleus of infected cells to inhibit the PolII cofactor RBP1 and attenuate global transcription as a potent immune evasion strategy (Akhrymuk et al., 2012, 2019). Disruption of canonical PolII complexes has been shown to result in a redistribution of PolII to lncRNA loci (Nojima et al., 2018). Thus, it is possible that alphaviral nsp2-mediated transcriptional shutoff results in an indirect induction of *ALPHA*. Future work will focus on defining the molecular signal that drives *ALPHA* upregulation during infection.

Much of our current understanding of innate immune-associated lncRNAs has focused on nuclear-resident lncRNAs that regulate immune gene expression. We found that *ALPHA*, which is localized in the cytoplasm, can bind directly to CHIKV genomic RNA establishing a new paradigm. How the *ALPHA*-CHIKV RNA interaction attenuates viral replication is still unclear. Alignment studies between full-length *ALPHA* and CHIKV genomic RNA did not reveal obvious regions of extensive complementarity (data not shown). However, previous work has shown that functional RNA-RNA interactions can be formed between short, tiled sequences (Lee et al., 2015). More restricted analysis of CHIKV nsp1 and *ALPHA* ex1 reveal two, consecutive, tiled, 7-nt regions of complementarity within the first 100 nt of *ALPHA* and nucleotides 380–490 of CHIKV nsp1 (Figures S7B and S7C). Although the second of these sites (starting at nucleotide 484) is similarly conserved across alphaviruses, the first site spanning nucleotides 380–386 is highly conserved in ONNV (~86%) but poorly conserved in MAYV (~29%) and absent in SINV (Figure S7C). Since *ALPHA* also controls ONNV, our data suggest that regions of similarity between these viruses are targeted. In addition to nucleotides 380–386, comparison of the full nsp1 sequence between related alphaviruses uncovered a region at the 3′ end that displays relatively high conservation with ONNV (78.9%), reduced conservation with MAYV (60.9%), and no conservation with SINV (Figure S7B). Notably, this region contains a mapped structural element in CHIKV spanning nucleotides 1,377–1,506

whose function remains unclear (Madden et al., 2020). Further analysis of the sequences underlying this structure reveals gaps in the MAYV genome at the 3′ end of this region but not in ONNV; this could consequently result in mismatched pairing and altered structure that may potentially affect *ALPHA* binding (Figure S7D). Indeed, given the highly structured nature of the CHIKV genome, the *ALPHA*-CHIKV RNA interaction may be mediated by secondary structure-to-structure contacts (Kendall et al., 2019; Madden et al., 2020). Although we found that the 3′ end of *ALPHA* ex1 is required for binding to CHIKV RNA, it remains unclear whether this is sequence dependent. Predicted secondary structures of both full-length and truncated *ALPHA* ex1 generated using RNAfold show that truncated ex1 remains highly structured but lacks a stem loop present in full-length ex1 (Figures S7E and S7F). It is possible that this stem loop is required for engagement with CHIKV RNA.

Together, our results provide evidence that cytoplasmic lncRNAs can have direct antiviral activity against closely related viruses. Furthermore, we demonstrate that a host lncRNA can physically interact with viral genomes to disrupt viral replication. More broadly, these findings may indicate an important role for lncRNAs as direct, antiviral effectors which complement canonical innate immune signaling pathways to control infection. Indeed, lncRNAs may be uniquely suited to this function as they are subject to reduced selective pressure relative to coding genes allowing for more rapid acquisition of immune activity in the context of the ever-present evolutionary arms race between host and virus. Our observation that infection-dependent lncRNA induction is also virus specific further supports the hypothesis that lncRNAs may represent a new avenue to discover antiviral RNAs. Future studies will define the full spectrum of lncRNAs that like *ALPHA* serve as important antiviral effectors that can function independently of canonical IFN-mediated innate immune responses to directly inhibit infection.

Limitations of the study

Although our results demonstrate that *ALPHA* binds CHIKV genomic RNA, we have not definitively linked this interaction to the inhibition of CHIKV replication. Furthermore, the exact molecular signal that drives *ALPHA* induction following alphavirus infection has yet to be defined.

STAR★METHODS

Detailed methods are provided in the online version of this paper and include the following:

SUPPLEMENTAL INFORMATION

Supplemental information can be found online at https://doi.org/10.1016/j.molcel.2022.08.030.

ACKNOWLEDGMENTS

We thank the Cherry, Henao-Mejia, Liu, Lynch, and Beiting labs for scientific discussion and assistance with data analysis, assays, and reagents. We thank the High Throughput Screening Core at the University of Pennsylvania for technical support with the lncRNA screens. We thank C. Coyne for HBMEC and HSV-1-GFP, M. Heise for CHIKV-mKate and SINV-mKate, D. Weiner for CHIKV, T.E. Morrison for ONNV, M. Diamond for MAYV, ZIKV, RVFV, and LACV, R. Kuhn for RRV-GFP, and S. Hensley for IAV. We thank Y. Loo and M. Gale for the IFNβ-mCherry plasmid and Addgene for lentivirus and CRISPR plasmids. Funding: this work was supported by grants from the National Institutes of Health to S.C. (R01AI074951, R01AI122749, 1R21AI151882, and R01AI140539) and J.H.-M. (R21AI128060, R21DK111755, and RO1HL136572) as well as funding to S.C. from the Penn Center for Precision Medicine, Mercatus, and the Gates Foundation. J.H.-M. is a recipient of the P.E.W. Biomedical Scholars Award. S.C. and J.H.-M. are recipients of the Burroughs Wellcome Investigators in the Pathogenesis of Infectious Disease Award. Schematics in Figures 4, 5, S6, and S7 and the graphical abstract were generated using Biorender.com.

AUTHOR CONTRIBUTIONS

Conceptualization: M.G.B., J.H.-M., and S.C.; methodology: M.G.B., J.H.-M., and S.C.; formal analysis: M.G.B. and M.F.; investigation: M.G.B., M.D., M.C.S., K.W., J.S., and H.S.; writing-original draft: M.G.B., J.H.-M., and S.C.; writing-review and editing: M.G.B., J.H.-M., and S.C.; supervision: K.F.L., D.P.B., K.W.L., J.H.-M., and S.C.

DECLARATION OF INTERESTS

The authors declare no competing interests.

Received: October 4, 2021
Revised: July 6, 2022
Accepted: August 26, 2022
Published: September 26, 2022

REFERENCES

Agarwal, S., Vierbuchen, T., Ghosh, S., Chan, J., Jiang, Z., Kandasamy, R.K., Ricci, E., and Fitzgerald, K.A. (2020). The long non-coding RNA LUCAT1 is a negative feedback regulator of interferon responses in humans. Nat. Commun. *11*, 6348. https://doi.org/10.1038/s41467-020-20165-5.

Agliano, F., Rathinam, V.A., Medvedev, A.E., Vanaja, S.K., and Vella, A.T. (2019). Long noncoding RNAs in host-pathogen interactions. Trends Immunol. *40*, 492–510. https://doi.org/10.1016/j.it.2019.04.001.

Akhrymuk, I., Kulemzin, S.V., and Frolova, E.I. (2012). Evasion of the innate immune response: the Old World Alphavirus nsP2 protein induces rapid degradation of Rpb1, a catalytic subunit of RNA polymerase II. J. Virol. *86*, 7180–7191. https://doi.org/10.1128/JVI.00541-12.

Akhrymuk, I., Lukash, T., Frolov, I., and Frolova, E.I. (2019). Novel mutations in nsP2 abolish Chikungunya virus-induced transcriptional shutoff and make the virus less cytopathic without affecting its replication rates. J. Virol. *93*. https://doi.org/10.1128/JVI.02062-18.

Atianand, M.K., Caffrey, D.R., and Fitzgerald, K.A. (2017). Immunobiology of long noncoding RNAs. Annu. Rev. Immunol. *35*, 177–198. https://doi.org/10.1146/annurev-immunol-041015-055459.

Basavappa, M., Cherry, S., and Henao-Mejia, J. (2019). Long noncoding RNAs and the regulation of innate immunity and host-virus interactions. J. Leukoc. Biol. *106*, 83–93. https://doi.org/10.1002/JLB.3MIR0918-354R.

Bayer, A., Lennemann, N.J., Ouyang, Y., Bramley, J.C., Morosky, S., Marques, E.T., Jr., Cherry, S., Sadovsky, Y., and Coyne, C.B. (2016). Type III interferons produced by human placental trophoblasts confer protection against Zika virus infection. Cell Host Microbe *19*, 705–712. https://doi.org/10.1016/j.chom.2016.03.008.

Bick, M.J., Carroll, J.W., Gao, G., Goff, S.P., Rice, C.M., and MacDonald, M.R. (2003). Expression of the zinc-finger antiviral protein inhibits alphavirus replication. J. Virol. *77*, 11555–11562. https://doi.org/10.1128/jvi.77.21.11555-11562.2003.

Burt, F.J., Chen, W., Miner, J.J., Lenschow, D.J., Merits, A., Schnettler, E., Kohl, A., Rudd, P.A., Taylor, A., Herrero, L.J., et al. (2017). Chikungunya virus: an update on the biology and pathogenesis of this emerging pathogen. Lancet Infect. Dis. *17*, e107–e117. https://doi.org/10.1016/S1473-3099(16)30385-1.

Bushnell, B. (2022). BBMap. https://sourceforge.net/projects/bbmap/.

Cabili, M.N., Trapnell, C., Goff, L., Koziol, M., Tazon-Vega, B., Regev, A., and Rinn, J.L. (2011). Integrative annotation of human large intergenic noncoding RNAs reveals global properties and specific subclasses. Genes Dev. *25*, 1915–1927. https://doi.org/10.1101/gad.17446611.

Carpenter, S., and Fitzgerald, K.A. (2018). Cytokines and long noncoding RNAs. Cold Spring Harb. Perspect. Biol. *10*, a028589. https://doi.org/10.1101/cshperspect.a028589.

Chen, Y.G., Satpathy, A.T., and Chang, H.Y. (2017). Gene regulation in the immune system by long noncoding RNAs. Nat. Immunol. *18*, 962–972. https://doi.org/10.1038/ni.3771.

Chiappinelli, K.B., Strissel, P.L., Desrichard, A., Li, H., Henke, C., Akman, B., Hein, A., Rote, N.S., Cope, L.M., Snyder, A., et al. (2015). Inhibiting DNA methylation causes an interferon response in cancer via dsRNA including endogenous retroviruses. Cell *162*, 974–986. https://doi.org/10.1016/j.cell.2015.07.011.

Chow, K.T., Gale, M., Jr., and Loo, Y.M. (2018). RIG-I and other RNA sensors in antiviral immunity. Annu. Rev. Immunol. *36*, 667–694. https://doi.org/10.1146/annurev-immunol-042617-053309.

Chu, C., Quinn, J., and Chang, H.Y. (2012). Chromatin isolation by RNA purification (ChIRP). J. Vis. Exp. 3192.

Elling, R., Chan, J., and Fitzgerald, K.A. (2016). Emerging role of long noncoding RNAs as regulators of innate immune cell development and inflammatory gene expression. Eur. J. Immunol. *46*, 504–512. https://doi.org/10.1002/eji.201444558.

Fabregat, A., Jupe, S., Matthews, L., Sidiropoulos, K., Gillespie, M., Garapati, P., Haw, R., Jassal, B., Korninger, F., May, B., et al. (2018). The reactome pathway KnowledgeBase. Nucleic Acids Res. *46*, D649–D655. https://doi.org/10.1093/nar/gkx1132.

Fox, J.M., and Diamond, M.S. (2016). Immune-mediated protection and pathogenesis of Chikungunya virus. J. Immunol. *197*, 4210–4218. https://doi.org/10.4049/jimmunol.1601426.

Fredriksson, S., Gullberg, M., Jarvius, J., Olsson, C., Pietras, K., Gústafsdóttir, S.M., Ostman, A., and Landegren, U. (2002). Protein detection using proximity-dependent DNA ligation assays. Nat. Biotechnol. *20*, 473–477. https://doi.org/10.1038/nbt0502-473.

Fros, J.J., Liu, W.J., Prow, N.A., Geertsema, C., Ligtenberg, M., Vanlandingham, D.L., Schnettler, E., Vlak, J.M., Suhrbier, A., Khromykh, A.A., and Pijlman, G.P. (2010). Chikungunya virus nonstructural protein 2 inhibits type I/II interferon-stimulated JAK-STAT signaling. J. Virol. *84*, 10877–10887. https://doi.org/10.1128/JVI.00949-10.

Fros, J.J., Major, L.D., Scholte, F.E.M., Gardner, J., van Hemert, M.J., Suhrbier, A., and Pijlman, G.P. (2015). Chikungunya virus non-structural protein 2-mediated host shut-off disables the unfolded protein response. J. Gen. Virol. *96*, 580–589. https://doi.org/10.1099/vir.0.071845-0.

Fros, J.J., and Pijlman, G.P. (2016). Alphavirus infection: host cell shut-off and inhibition of antiviral responses. Viruses *8*, 166. https://doi.org/10.3390/v8060166.

Fros, J.J., van der Maten, E., Vlak, J.M., and Pijlman, G.P. (2013). The C-terminal domain of Chikungunya virus nsP2 independently governs viral RNA replication, cytopathicity, and inhibition of interferon signaling. J. Virol. *87*, 10394–10400. https://doi.org/10.1128/JVI.00884-13.

Göertz, G.P., McNally, K.L., Robertson, S.J., Best, S.M., Pijlman, G.P., and Fros, J.J. (2018). The methyltransferase-like domain of Chikungunya virus nsP2 inhibits the interferon response by promoting the nuclear export of STAT1. J. Virol. *92*, e01008-18. https://doi.org/10.1128/JVI.01008-18.

Gorbea, C., Mosbruger, T., and Cazalla, D. (2017). A viral Sm-class RNA base-pairs with mRNAs and recruits microRNAs to inhibit apoptosis. Nature *550*, 275–279. https://doi.org/10.1038/nature24034.

Gu, Z., Eils, R., and Schlesner, M. (2016). Complex heatmaps reveal patterns and correlations in multidimensional genomic data. Bioinformatics *32*, 2847–2849. https://doi.org/10.1093/bioinformatics/btw313.

Hadjicharalambous, M.R., and Lindsay, M.A. (2019). Long non-coding RNAs and the innate immune response. Noncoding. RNA *5*, 34. https://doi.org/10.3390/ncrna5020034.

Hon, C.C., Ramilowski, J.A., Harshbarger, J., Bertin, N., Rackham, O.J., Gough, J., Denisenko, E., Schmeier, S., Poulsen, T.M., Severin, J., et al. (2017). An atlas of human long non-coding RNAs with accurate 5′ ends. Nature *543*, 199–204. https://doi.org/10.1038/nature21374.

Hou, F., Sun, L., Zheng, H., Skaug, B., Jiang, Q.X., and Chen, Z.J. (2011). MAVS forms functional prion-like aggregates to activate and propagate antiviral innate immune response. Cell *146*, 448–461. https://doi.org/10.1016/j.cell.2011.06.041.

Howe, K.L., Achuthan, P., Allen, J., Allen, J., Alvarez-Jarreta, J., Amode, M.R., Armean, I.M., Azov, A.G., Bennett, R., Bhai, J., et al. (2021). Ensembl 2021. Nucleic Acids Res. *49*, D884–D891. https://doi.org/10.1093/nar/gkaa942.

Jiang, M., Zhang, S., Yang, Z., Lin, H., Zhu, J., Liu, L., Wang, W., Liu, S., Liu, W., Ma, Y., et al. (2018). Self-recognition of an inducible Host lncRNA by RIG-I Feedback Restricts Innate Immune Response. Cell *173*. 906.e13–919.e13. https://doi.org/10.1016/j.cell.2018.03.064.

Jones, J.E., Long, K.M., Whitmore, A.C., Sanders, W., Thurlow, L.R., Brown, J.A., Morrison, C.R., Vincent, H., Peck, K.M., Browning, C., et al. (2017). Disruption of the opal stop codon attenuates Chikungunya virus-induced arthritis and pathology. mBio *8*, e01456-17. https://doi.org/10.1128/mBio.01456-17.

Kearns, N.A., Genga, R.M., Enuameh, M.S., Garber, M., Wolfe, S.A., and Maehr, R. (2014). Cas9 effector-mediated regulation of transcription and differentiation in human pluripotent stem cells. Development *141*, 219–223. https://doi.org/10.1242/dev.103341.

Kelvin, A.A., Banner, D., Silvi, G., Moro, M.L., Spataro, N., Gaibani, P., Cavrini, F., Pierro, A., Rossini, G., Cameron, M.J., et al. (2011). Inflammatory cytokine expression is associated with Chikungunya virus resolution and symptom severity. PLoS Negl. Trop. Dis. *5*, e1279. https://doi.org/10.1371/journal.pntd.0001279.

Kendall, C., Khalid, H., Müller, M., Banda, D.H., Kohl, A., Merits, A., Stonehouse, N.J., and Tuplin, A. (2019). Structural and phenotypic analysis of Chikungunya virus RNA replication elements. Nucleic Acids Res. *47*, 9296–9312. https://doi.org/10.1093/nar/gkz640.

Kotzin, J.J., Spencer, S.P., McCright, S.J., Kumar, D.B.U., Collet, M.A., Mowel, W.K., Elliott, E.N., Uyar, A., Makiya, M.A., Dunagin, M.C., et al. (2016). The long non-coding RNA Morrbid regulates Bim and short-lived myeloid cell lifespan. Nature *537*, 239–243. https://doi.org/10.1038/nature19346.

Lee, N., Moss, W.N., Yario, T.A., and Steitz, J.A. (2015). EBV noncoding RNA binds nascent RNA to drive host PAX5 to viral DNA. Cell *160*, 607–618. https://doi.org/10.1016/j.cell.2015.01.015.

Lin, H., Jiang, M., Liu, L., Yang, Z., Ma, Z., Liu, S., Ma, Y., Zhang, L., and Cao, X. (2019). The long noncoding RNA Lnczc3h7a promotes a TRIM25-mediated RIG-I antiviral innate immune response. Nat. Immunol. *20*, 812–823. https://doi.org/10.1038/s41590-019-0379-0.

Long, K.M., Ferris, M.T., Whitmore, A.C., Montgomery, S.A., Thurlow, L.R., McGee, C.E., Rodriguez, C.A., Lim, J.K., and Heise, M.T. (2016). γδ T cells play a protective role in Chikungunya virus-induced disease. J. Virol. *90*, 433–443. https://doi.org/10.1128/JVI.02159-15.

Love, M.I., Huber, W., and Anders, S. (2014). Moderated estimation of fold change and dispersion for RNA-seq data with DESeq2. Genome Biol. *15*, 550. https://doi.org/10.1186/s13059-014-0550-8.

Ma, D.Y., and Suthar, M.S. (2015). Mechanisms of innate immune evasion in re-emerging RNA viruses. Curr. Opin. Virol. *12*, 26–37. https://doi.org/10.1016/j.coviro.2015.02.005.

MacDonald, M.R., Machlin, E.S., Albin, O.R., and Levy, D.E. (2007). The zinc finger antiviral protein acts synergistically with an interferon-induced factor for maximal activity against alphaviruses. J. Virol. *81*, 13509–13518. https://doi.org/10.1128/JVI.00402-07.

Madden, E.A., Plante, K.S., Morrison, C.R., Kutchko, K.M., Sanders, W., Long, K.M., Taft-Benz, S., Cruz Cisneros, M.C., White, A.M., Sarkar, S., et al. (2020). Using SHAPE-MaP to model RNA secondary structure and identify 3′UTR variation in Chikungunya virus. J. Virol. *94*, e00701-20. https://doi.org/10.1128/JVI.00701-20.

Matusali, G., Colavita, F., Bordi, L., Lalle, E., Ippolito, G., Capobianchi, M.R., and Castilletti, C. (2019). Tropism of the Chikungunya virus. Viruses *11*, 175. https://doi.org/10.3390/v11020175.

Meertens, L., Hafirassou, M.L., Couderc, T., Bonnet-Madin, L., Kril, V., Kümmerer, B.M., Labeau, A., Brugier, A., Simon-Loriere, E., Burlaud-Gaillard, J., et al. (2019). FHL1 is a major host factor for Chikungunya virus infection. Nature *574*, 259–263. https://doi.org/10.1038/s41586-019-1578-4.

Meshram, C.D., Lukash, T., Phillips, A.T., Akhrymuk, I., Frolova, E.I., and Frolov, I. (2019). Lack of nsP2-specific nuclear functions attenuates Chikungunya virus replication both in vitro and in vivo. Virology *534*, 14–24. https://doi.org/10.1016/j.virol.2019.05.016.

Mimee, M., Tucker, A.C., Voigt, C.A., and Lu, T.K. (2015). Programming a human commensal Bacterium, *Bacteroides thetaiotaomicron*, to sense and respond to stimuli in the murine gut microbiota. Cell Syst. *1*, 62–71. https://doi.org/10.1016/j.cels.2015.06.001.

Moser, L.A., Ramirez-Carvajal, L., Puri, V., Pauszek, S.J., Matthews, K., Dilley, K.A., Mullan, C., McGraw, J., Khayat, M., Beeri, K., et al. (2016). A universal next-generation sequencing protocol to generate noninfectious barcoded cDNA libraries from high-containment RNA viruses. mSystems *1*, e00039-15. https://doi.org/10.1128/mSystems.00039-15.

Mowel, W.K., Kotzin, J.J., McCright, S.J., Neal, V.D., and Henao-Mejia, J. (2018). Control of immune cell homeostasis and function by lncRNAs. Trends Immunol. *39*, 55–69. https://doi.org/10.1016/j.it.2017.08.009.

Mowel, W.K., McCright, S.J., Kotzin, J.J., Collet, M.A., Uyar, A., Chen, X., DeLaney, A., Spencer, S.P., Virtue, A.T., Yang, E., et al. (2017). Group 1 innate lymphoid cell lineage identity is determined by a cis-regulatory element marked by a long non-coding RNA. Immunity *47*. 435.e8–449.e8. https://doi.org/10.1016/j.immuni.2017.08.012.

Nayak, T.K., Mamidi, P., Sahoo, S.S., Kumar, P.S., Mahish, C., Chatterjee, S., Subudhi, B.B., Chattopadhyay, S., and Chattopadhyay, S. (2019). P38 and JNK mitogen-activated protein kinases interact with Chikungunya virus non-structural Protein-2 and regulate TNF induction during viral infection in macrophages. Front. Immunol. *10*, 786. https://doi.org/10.3389/fimmu.2019.00786.

Nelemans, T., and Kikkert, M. (2019). Viral innate immune evasion and the pathogenesis of emerging RNA virus infections. Viruses *11*, 961. https://doi.org/10.3390/v11100961.

Ng, L.F., Chow, A., Sun, Y.J., Kwek, D.J., Lim, P.L., Dimatatac, F., Ng, L.C., Ooi, E.E., Choo, K.H., Her, Z., et al. (2009). IL-1beta, IL-6, and RANTES as biomarkers of chikungunya severity. PLoS One *4*, e4261. https://doi.org/10.1371/journal.pone.0004261.

Nojima, T., Tellier, M., Foxwell, J., Ribeiro de Almeida, C., Tan-Wong, S.M., Dhir, S., Dujardin, G., Dhir, A., Murphy, S., and Proudfoot, N.J. (2018). Deregulated expression of mammalian lncRNA through loss of SPT6 induces R-loop formation, replication stress, and cellular senescence. Mol. Cell *72*. 970.e7–984.e7. https://doi.org/10.1016/j.molcel.2018.10.011.

Patro, R., Duggal, G., Love, M.I., Irizarry, R.A., and Kingsford, C. (2017). Salmon provides fast and bias-aware quantification of transcript expression. Nat. Methods *14*, 417–419. https://doi.org/10.1038/nmeth.4197.

Reed, L.J., and Muench, H. (1938). A simple method of estimating fifty per cent endpoints12. Am. J. Epidemiol. *27*, 493–497.

Rehwinkel, J., and Gack, M.U. (2020a). RIG-I-like receptors: their regulation and roles in RNA sensing. Nat. Rev. Immunol. *20*, 537–551. https://doi.org/10.1038/s41577-020-0288-3.

Sanjana, N.E., Shalem, O., and Zhang, F. (2014). Improved vectors and genome-wide libraries for CRISPR screening. Nat. Methods *11*, 783–784. https://doi.org/10.1038/nmeth.3047.

Schneider, W.M., Chevillotte, M.D., and Rice, C.M. (2014). Interferon-stimulated genes: a complex web of host defenses. Annu. Rev. Immunol. *32*, 513–545. https://doi.org/10.1146/annurev-immunol-032713-120231.

Schoggins, J.W. (2019). Interferon-stimulated genes: what do they all do? Annu. Rev. Virol. *6*, 567–584. https://doi.org/10.1146/annurev-virology-092818-015756.

Schwartz, O., and Albert, M.L. (2010). Biology and pathogenesis of Chikungunya virus. Nat. Rev. Microbiol. *8*, 491–500. https://doi.org/10.1038/nrmicro2368.

Seth, R.B., Sun, L., Ea, C.K., and Chen, Z.J. (2005). Identification and characterization of MAVS, a mitochondrial antiviral signaling protein that activates NF-kappaB and IRF 3. Cell *122*, 669–682. https://doi.org/10.1016/j.cell.2005.08.012.

Shalem, O., Sanjana, N.E., Hartenian, E., Shi, X., Scott, D.A., Mikkelson, T., Heckl, D., Ebert, B.L., Root, D.E., Doench, J.G., and Zhang, F. (2014). Genome-scale CRISPR-Cas9 knockout screening in human cells. Science *343*, 84–87. https://doi.org/10.1126/science.1247005.

Silva, L.A., and Dermody, T.S. (2017). Chikungunya virus: epidemiology, replication, disease mechanisms, and prospective intervention strategies. J. Clin. Invest. *127*, 737–749. https://doi.org/10.1172/JCI84417.

Söderberg, O., Gullberg, M., Jarvius, M., Ridderstråle, K., Leuchowius, K.J., Jarvius, J., Wester, K., Hydbring, P., Bahram, F., Larsson, L.G., and Landegren, U. (2006). Direct observation of individual endogenous protein complexes in situ by proximity ligation. Nat. Methods *3*, 995–1000. https://doi.org/10.1038/nmeth947.

Solignat, M., Gay, B., Higgs, S., Briant, L., and Devaux, C. (2009). Replication cycle of chikungunya: a re-emerging arbovirus. Virology *393*, 183–197. https://doi.org/10.1016/j.virol.2009.07.024.

Soneson, C., Love, M.I., and Robinson, M.D. (2015). Differential analyses for RNA-seq: transcript-level estimates improve gene-level inferences. F1000Res *4*, 1521. https://doi.org/10.12688/f1000research.7563.2.

RCoreTeam (2018). R: A language and environment for statistical computing. (The R Foundation). https://www.r-project.org/.

Stewart, C.E., Randall, R.E., and Adamson, C.S. (2014). Inhibitors of the interferon response enhance virus replication in vitro. PLoS One *9*, e112014. https://doi.org/10.1371/journal.pone.0112014.

Tanabe, I.S.B., Tanabe, E.L.L., Santos, E.C., Martins, W.V., Araújo, I.M.T.C., Cavalcante, M.C.A., Lima, A.R.V., Câmara, N.O.S., Anderson, L., Yunusov, D., and Bassi, Ê.J. (2018). Cellular and molecular immune response to Chikungunya virus infection. Front. Cell. Infect. Microbiol. *8*, 345. https://doi.org/10.3389/fcimb.2018.00345.

Ullah, M.O., Sweet, M.J., Mansell, A., Kellie, S., and Kobe, B. (2016). TRIF-dependent TLR signaling, its functions in host defense and inflammation, and its potential as a therapeutic target. J. Leukoc. Biol. *100*, 27–45. https://doi.org/10.1189/jlb.2RI1115-531R.

Varghese, F.S., Thaa, B., Amrun, S.N., Simarmata, D., Rausalu, K., Nyman, T.A., Merits, A., McInerney, G.M., Ng, L.F.P., and Ahola, T. (2016). The antiviral alkaloid berberine reduces Chikungunya virus-induced mitogen-activated protein kinase signaling. J. Virol. *90*, 9743–9757. https://doi.org/10.1128/JVI.01382-16.

Venugopalan, A., Ghorpade, R.P., and Chopra, A. (2014). Cytokines in acute chikungunya. PLoS One *9*, e111305. https://doi.org/10.1371/journal.pone.0111305.

Vierbuchen, T., and Fitzgerald, K.A. (2021). Long non-coding RNAs in antiviral immunity. Semin. Cell Dev. Biol. *111*, 126–134. https://doi.org/10.1016/j.semcdb.2020.06.009.

Wang, P., Xue, Y., Han, Y., Lin, L., Wu, C., Xu, S., Jiang, Z., Xu, J., Liu, Q., and Cao, X. (2014). The STAT3-binding long noncoding RNA lnc-DC controls human dendritic cell differentiation. Science *344*, 310–313. https://doi.org/10.1126/science.1251456.

Ward, J.H. (1963). Hierarchical grouping to optimize an objective function. J. Am. Stat. Assoc. *58*, 236–244. https://doi.org/10.2307/2282967.

Werner, M.S., Sullivan, M.A., Shah, R.N., Nadadur, R.D., Grzybowski, A.T., Galat, V., Moskowitz, I.P., and Ruthenburg, A.J. (2017). Chromatin-enriched lncRNAs can act as cell-type specific activators of proximal gene transcription. Nat. Struct. Mol. Biol. *24*, 596–603. https://doi.org/10.1038/nsmb.3424.

Wickham, H., Francois, R., Henry, L., and Müller, K. (2017). dplyr: a grammar of data manipulation. https://joss.theoj.org/papers/10.21105/joss.01686.

Yi, K., Zhang, Y., Wang, Y., Wang, Z., Xie, M., Jin, Z., and Zhao, T. (2019). Long noncoding RNA and its role in virus infection and pathogenesis. Front. Biosci. (Landmark Ed.) *24*, 777–789.

Zhang, W., Xie, M., Shu, M.D., Steitz, J.A., and DiMaio, D. (2016). A proximity-dependent assay for specific RNA-protein interactions in intact cells. RNA *22*, 1785–1792. https://doi.org/10.1261/rna.058248.116.

STAR★METHODS

KEY RESOURCES TABLE

REAGENT or RESOURCE	SOURCE	IDENTIFIER
Antibodies		
Anti-IFIT1 (D2X9Z)	Cell Signaling	Cat#14769S; RRID:AB_2783869
Anti-dsRNA (J2)	Cherry Laboratory	N/A
Anti-CHIKV E2	Dr. Michael Diamond, Washington University in St. Louis	N/A
Anti-IAV NP	Dr. Scott Hensley, University of Pennsylvania	N/A
Streptavidin-HRP	Cell Signaling	Cat#3999S; RRID:AB_10830897
Bacterial and virus strains		
CHIKV	Dr. David Weiner, University of Pennsylvania	N/A
CHIKV-mKate (181/25)	Dr. Mark Heise, University of North Carolina	N/A
ONNV (SG650)	Dr. Thomas E. Morrison, University of Colorado	N/A
MAYV (BeH407)	Dr. Michael Diamond, Washington University in St. Louis	N/A
RRV-GFP	Dr. R. Kuhn, Purdue University of Pennsylvania	N/A
SINV-mKate (Girdwood)	Dr. Mark Heise, University of North Carolina	N/A
ZIKV (MR766)	Dr. Michael Diamond, Washington University in St. Louis	N/A
RVFV (MP12)	Dr. Michael Diamond, Washington University in St. Louis	N/A
LACV	Dr. Michael Diamond, Washington University in St. Louis	N/A
IAV (A/Puerto Rico/8/34)	Dr. Scott Hensley, University of Pennsylvania	N/A
SeV (Cantelli)	Charles River Laboratories	Cat#10100774
HSV-1-GFP	Dr. Carolyn Coyne, University of Pittsburgh	N/A
One Shot Stbl3 Chemically Competent Cells	Thermo Fisher	Cat#C737303
Chemicals, peptides, and recombinant proteins		
Cycloheximide	Sigma Aldrich	Cat#01810
Recombinant human IFNβ	Peprotech	Cat#300-02BC
Recombinant human IL-1β	Peprotech	Cat#200-01B
Recombinant human TNFα	Peprotech	Cat#300-01A
Ruxolitinib	Invivogen	Cat#tlrl-rux
AL8810	Santa Cruz Biotechnologies	Cat#sc-205204
SP600125	Invivogen	Cat#tlrl-sp60
PD98095	Invivogen	Cat#tlrl-pd98
Ionomycin	Sigma-Aldrich	Cat#I0634
TRIzol	Life Technologies	Cat#15596018
HiPerfect	Qiagen	Cat#301705
Lipofectamine 2000	Invitrogen	Cat#11668-019
Polybrene	Fisher Scientific	Cat#TR1003G
Puromycin	Takara Bio	Cat#63130
G418	Cell Center, University of Pennsylvania	N/A
DYNAL MyOne Dynabeads Streptavidin C1	Thermo Fisher	Cat#65-001
Hybond-N+ Membrane	GE Healthcare	Cat#RPN303B

(*Continued on next page*)

Continued

REAGENT or RESOURCE	SOURCE	IDENTIFIER
ECL	Amersham	Cat#GERPN2106
Metaphor Agarose	Fisher Scientific	Cat#BMA50181
Ethidium Bromide	Sigma-Aldrich	Cat#E1510
Quick-Load Purple 2-Log Ladder	New England Biotechnologies	Cat#N0550
T4 DNA Ligase	New England Biotechnologies	Cat#M0202
Phi29 Polymerase	New England Biotechnologies	Cat#M0269
Vectashield	Fisher Scientific	Cat#NC9265087
Critical commercial assays		
RNA Clean and Concentrator Kit	Zymogen Research	Cat#R1018
M-MLV Reverse Transcriptase	Life Technologies	Cat#28025021
Power SYBR Green PCR MasterMix	Life Technologies	Cat#4368708
TruSeq Stranded Total RNA Kit	Illumina	Cat#20020596
Phusion High Fidelity DNA Polymerase Kit	New England Biotechnologies	Cat#M0530
RNA 3' End Biotinylation Kit	Thermo Fisher	Cat#20160
T7 MEGAscript Kit	Life Technologies	Cat#AMB13345
SP6 MEGAscript Kit	Thermo Fisher	Cat#AM1330
Deposited data		
RNA-seq datasets	This paper	GSE184306
Microscope images	Mendeley	https://data.mendeley.com/datasets/yxxg7x5c6y/draft?a=28296dfe-76bf-448c-8a94-662582b96df6
Experimental models: cell lines		
HBMEC	Dr. Carolyn Coyne, University of Pittsburgh	N/A
BHK-21	ATCC	CCL-10; **RRID:CVCL_1915**
Vero	ATCC	CCL-81; **RRID:CVCL_0059**
U2OS	ATCC	HTB-96; **RRID:CVCL_0042**
HEK293T	ATCC	CRL-3216; **RRID:CVCL_0063**
Primary Human Peripheral Blood Monocytes	Human Immunology Core, University of Pennsylvania	N/A
Recombinant dna		
lentiCRISPRv2-Puro	Addgene	98290; **RRID:Addgene_98290**
pLenti-Puro	Addgene	39481; **RID:Addgene_39481**
psPAX2	Addgene	12260; **RRID:Addgene_12260**
pCMV-VSV-G	Addgene	8454; **RRID:Addgene_8454**
pcDNA3(+)-ALPHA	This paper (generated by Genscript)	N/A
pJMH40-CHIKV Replicon	Dr. Mark Heise, University of North Carolina	N/A
Oligonucleotides		
qPCR: CHIKVnsp2-F: GGCAGTGGTCCCAGATAATTCAAG	This paper	N/A
qPCR: CHIKVnsp2-R: ACTGTCTAGATCCACCCCATACATG	This paper	N/A
qPCR: ALPHA-F: CCTTGCTGCCCTCATGATAATTC	This paper	N/A
qPCR: ALPHA-R: TCACAGCAGGACACACTATG	This paper	N/A
qPCR: GAPDH-F: ACCAAATCCGTTGACTCCGACCTT	This paper	N/A
qPCR: GAPDH-R: TCGACAGTCAGCCGCATCTTCTTT	This paper	N/A

(*Continued on next page*)

Continued

REAGENT or RESOURCE	SOURCE	IDENTIFIER
qPCR: IFNB1-F: GCTTCTCCACTACAGCTCTTTC	This paper	N/A
qPCR: IFNB1-R: CAGTATTCAAGCCTCCCATTCA	This paper	N/A
qPCR: ISG56-F: CAACCAAGCAAATGTGAGGA	This paper	N/A
qPCR: ISG56-R: AGGGGAAGCAAAGAAAATGG	This paper	N/A
qPCR: NEAT1-F: GATCTTTTCCACCCCAAGAGTACATAA	This paper	N/A
qPCR: NEAT1-R: CTCACACAAACACAGATTCCACAAC	This paper	N/A
qPCR: MALAT1-F: TTCCGGGTGTTGTAGGTTTC	This paper	N/A
qPCR: MALAT1-R: AAACCCACAAACTTGCCATC	This paper	N/A
qPCR: CHIKV Anti-Genome cDNA Primer: GGCAGTATCGTGAATTCGATGCCG CTGTACCGTCCCCATTCC	Meertens et al., 2019	N/A
qPCR: CHIKV Anti-Genome-F: GGCAGTATCGTGAATTCGATGC	Meertens et al., 2019	N/A
qPCR: CHIKV Anti-Genome-R: ACTGCTGAGTCCAAAGTGGG	Meertens et al., 2019	N/A
qPCR: gBlock CHIKV Anti-Genome Amplicon Standard:GGCAGTATCGTGA ATTCGATGCCGCTGTACCGTCCCCAT TCCAGAACACACTACAGAATGTACTG GCAGCAGCCACGAAAAGAAACTGCAA CGTCACACAGATGAGGGAATTCACCA CTTTGGACTCAGCAGT	Meertens et al., 2019	N/A
RNA-PLA: CHIKV-NonPriming: AGAGACATAGCTGTGTCAC GCGTCTCCGCTGTTTCTTGT AAAAAAAAAAAAAAAAAGACG CTAATAGTTAAGACGCTT [UUU]	This paper	N/A
RNA-PLA: CHIKV50bpdown-Priming: TTGGTGCACCGAAGGAGAT CGGCGGGTGACTCAGTTC CGTAAAAAAAAAAAAAAAA AAATATGACAGAACTAGACACTCTT	This paper	N/A
RNA-PLA: ALPHA-Priming: TCACAGCAGGACACACTAT GTAATTCATATCAACATTTGG GAAAAAAAAAAAAAAAAA AATATGACAGAACTAGACACTCTT	This paper	N/A
RNA-PLA: GAPDH-Priming: GCTGGCGACGCAAAAGAA GATGCGGCTGACTGTCGA ACAGAAAAAAAAAAAAAAAAA AATATGACAGAACTAGACACTCTT	This paper	N/A
RNA-PLA: Connector: CTATTAGCGTCCAGTGAATG CGAGTCCGTCTAAGAGAGT AGTACAGCAGCCGTCAAGAGTGTCTA	Söderberg et al., 2006	N/A
RNA-PLA: Linker: GTTCTGTCATATTTAAGCGTCTTAA	Söderberg et al., 2006	N/A

(*Continued on next page*)

Continued

REAGENT or RESOURCE	SOURCE	IDENTIFIER
RNA-PLA: Amplicon Probe: /5Cy5/CAGTGAATGCGAGTCCGTCT	Söderberg et al., 2006	N/A
ChIRP/IVP: CHIKVnsp3probe-F: TAATACGACTCACTATAGGGAG ACTGCGATATTGTTCGCGTGC	This paper	N/A
ChIRP/IVP: CHIKVnsp3oprobe-R: ATTTAGGTGACACTATAGAAGG GACGTGATTGTACTCGCCTCC	This paper	N/A
ChIRP: SINVnsp3probe-F: TAATACGACTCACTATAGGGAG AGAAAGTGATCCACGCGGTTG	This paper	N/A
ChIRP: SINVnsp3probe-R: ATTTAGGTGACACTATAGAAGG GGCTCGTTGCTTTCCTGGTCA	This paper	N/A
ChIRP: GAPDHprobe-F: TAATACGACTCACTATAGGGA GAATCTTCTTTTGCGTCGCCAG	This paper	N/A
ChIRP:GAPDHprobe-R: ATTTAGGTGACACTATAGAAGG GTGCAGGAGGCATTGCTGATG	This paper	N/A
IVP: GAPDHprobe-F: TAATACGACTCACTATAGGGAG AAAAATCAAGTGGGGCGATGC	This paper	N/A
IVP: GAPDHprobe-R: ATTTAGGTGACACTATAGAAGG GTCTAGACGGCAGGTCAGGTC	This paper	N/A
IVP: ALPHAprobe-F: TAATACGACTCACTATAGGG AGAATTTGGCTCTGTGTCCCTA	This paper	N/A
IVP: ALPHAprobe-R: ATTTAGGTGACACTATAGAAG GGTCATAATCCCCGGTGTTGG	This paper	N/A
IVP: ALPHA5Pprobe-F: TAATACGACTCACTATAGGGAG AATTTGGCTCTGTGTCCCTAC	This paper	N/A
IVP: ALPHA5Pprobe-R: TATATAGCCTTCTGATGCTC	This paper	N/A
IVP: ALPHA3Pprobe-F: TAATACGACTCACTATAGGGAG AACCTGCTCAGATTCTGGGAAG	This paper	N/A
IVP: ALPHA3Pprobe-R: CGGTGTTGGGGGTGGAACC	This paper	N/A
IVP: ALPHAMidprobe-F: TAATACGACTCACTATAGGGAG ACCTTGCTGCCCTCATGATAA	This paper	N/A
IVP: ALPHAMidprobe-R: TTTAAAAATCTGTAGTACC	This paper	N/A
IVP: ALPHAEx1probe-R: TATCATGAGGGCAGCAAG	This paper	N/A
IVP: ALPHAEx2probe-F: TAATACGACTCACTATAGGGAG AATTCTGTGTTCAGTCAAAATAG	This paper	N/A
IVP: ALPHAEx2probe-R: CTTCTGATGCTCACAGCAG	This paper	N/A

(*Continued on next page*)

Continued

REAGENT or RESOURCE	SOURCE	IDENTIFIER
IVP: ALPHAEx1truncprobe-R: GAAAATCTGCCCCCGTGATC	This paper	N/A
IVP: CHIKVnsp1(SL15649)-F: TAATACGACTCACTATAGGGAG AATGGATCCTGTGTACGTGGAC	This paper	N/A
IVP: CHIKVnsp1(SL15649)-R: TGCGCCCGCTCTGTCCTCAAGC	This paper	N/A
IVP: CHIKVnsp2(SL15649)-F: TAATACGACTCACTATAGGGAGAG GAATAATAGAGACTCCGAGAGG	This paper	N/A
IVP: CHIKVnsp2(SL15649)-R: ACATCCTGCTCGGGTGACCTG	This paper	N/A
IVP: CHIKVnsp3(SL15649)-F: TAATACGACTCACTATAGGGAG AGCACCGTCGTACCGGGTAAAAC	This paper	N/A
IVP: CHIKVnsp3(SL15649)-R: CCACCTGCCCTGTCTAGTC	This paper	N/A
IVP: CHIKVnsp4(SL15649)-F: TAATACGACTCACTATAGGGAG ATATATATTCTCGTCGGACACCG	This paper	N/A
IVP: CHIKVnsp4(SL15649)-R: TTTAGGACCGCCGTACAAAG	This paper	N/A
CRISPR: sgControl1-S: CACCGTTCCGCGTTACATAACTTA	Kearns et al., 2014	N/A
CRISPR: sgControl1-AS: AAACTAAGTTATGTAACGCGGAAC	Kearns et al., 2014	N/A
CRISPR: sgControl2-S: CACCCTGGAATGAATTGGCCTATG	Mimee et al., 2015	N/A
CRISPR: sgControl2-AS: AAACCATAGGCCAATTCATTCCAG	Mimee et al., 2015	N/A
CRISPR: sgALPHA-5Prime-S: CACCGCAAAACACCCCTTCTCTAT	This paper	N/A
CRISPR: sgALPHA-5Prime-AS: AAACATAGAGAAGGGGTGTTTTGC	This paper	N/A
CRISPR: sgALPHA-3Prime-S: CACCGATGTTAGTGGTGTAGCTCTA	This paper	N/A
CRISPR: sgALPHA-3Primer-AS: AAACTAGAGCTACACCACTAACATC	This paper	N/A
Software and algorithms		
ImageJ	Wayne Rasband (NIH)	https://imagej.nih.gov/ij/
MetaXpress	Molecular Devices	N/A

RESOURCE AVAILABILITY

Lead contact

Questions and requests for reagents should be directed to and will be fulfilled by the lead contact Sara Cherry (cherrys@pennmedicine.upenn.edu).

Materials availability

Reagents generated within this study are available upon reasonable request to the Lead Contact.

Data and code availability

- All sequencing data generated in this manuscript are available through NCBI Gene Expression Omnibus: GSE184306.

- All unprocessed images can be found at the following link. Mendeley Data: https://data.mendeley.com/datasets/yxxg7x5c6y/draft?a=28296dfe-76bf-448c-8a94-662582b96df6.
- This paper does not report original code.
- Any additional information required to reanalyze data reported in this paper can be requested from the Lead Contact.

EXPERIMENTAL MODEL AND SUBJECT DETAILS

Cells and Viruses

Human brain microvascular endothelial cells (HBMEC) (Bayer et al., 2016) were maintained in Roswell Park Memorial Institute 1640 medium (RPMI 1640 with L-glutamine, Corning) containing 10% fetal bovine serum (FBS, Hyclone), 10% Nu-Serum (Corning), 1% penicillin/streptomycin (Sigma), 1% sodium pyruvate (Sigma), 1% non-essential amino acids (Sigma), 1% MEM vitamins (Sigma), and 10 μg/mL endothelial cell growth supplement (Corning). BHK-21, Vero, A549, U2OS, and HEK293T cells were acquired from American Type Culture Collections (ATCC) and cultured in Dulbecco's Modified Eagle's Medium (DMEM) containing 10% FBS, 1% P/S, and 0.5% L-glutamine. Primary human monocytes were isolated from patient blood by the University of Pennsylvania Human Immunology Core and cultured in RPMI 1640 (w/ L-glutamine) containing 10% FBS, and 1% P/S for a maximum length of 48h. All cell lines were confirmed mycoplasma-negative.

Chikungunya (CHIKV)-mKate (strain 181/25) and Sindbis (SINV)-mKate (strain Girdwood) were provided by Dr. Mark Heise (University of North Carolina). CHIKV (strain Ross) was provided by Dr. David Weiner (University of Pennsylvania). O'nyong'nyong (ONNV, strain SG650) was a gift from Dr. Thomas E. Morrison (University of Colorado). Mayaro (MAYV, strain BeH407), Zika (ZIKV, strain MR766), Rift Valley Fever (RVFV, strain MP12), and La Crosse (LACV) were gifts from Dr. Michael Diamond (Washington University in St. Louis). Ross River (RRV)-GFP was a gift from Dr. Richard Kuhn (Purdue University). Influenza A (IAV, strain A/Puerto Rico/8/34) was a gift from Dr. Scott Hensley (University of Pennsylvania). Sendai (SeV, strain Cantelli) was acquired from Charles River Laboratories (#10100774). Herpes Simplex (HSV)-1-GFP was a gift from Dr. Carolyn Coyne (University of Pittsburgh). CHIKV, SINV, MAYV, and ZIKV were all propagated in C636 mosquito cells. ONNV, RRV and HSV-1 were propagated in Vero-E6 cells. RVFV and LACV were propagated in BHK-21 cells. Supernatants from infected C636, Vero-E6, or BHK-21 cells were collected, aliquoted and subjected to only a single freeze-thaw. Titers (represented as pfu/mL) were calculated by plaque assays or $TCID_{50}$ assays performed on BHK-21 or Vero-E6 cells.

METHOD DETAILS

RNA-sequencing and analysis

HBMEC were either left uninfected (mock) or infected with CHIKV or ZIKV at MOI 5 for 24h. Cells were then directly lysed in TRIzol and RNA was extracted using the Zymogen RNA Clean and Concentrator Kit with on-column DNase I treatment. RNA quality was measured using the Agilent BioAnalyzer and quantified using the Qubit Fluorescent Quantification System (ThermoFisher Scientific). Libraries were prepared using the Illumina TruSeq Stranded Total RNA Kit with ribosomal RNA depletion. Paired-end sequencing with 150bp read-length was performed with the NextSeq 500.

Raw fastq files were trimmed to remove adapters and low quality reads with bbduk 38.56 using the parameters "ref=/bbmap/resources/adapters.fa ktrim=r k=23 mink=11 hdist=1 minlength=35 tpe tbo qtrim=r trimq=10" (Bushnell, 2022). Next transcripts were counted using salmon 0.13.1 in pseudoalignment mode by mapping to Homo sapiens (human) genome assembly GRCh38 (build 94) with the parameters "–validateMappings –rangeFactorizationBins 4 –seqBias –gcBias" (Patro et al., 2017). Transcript counts were collapsed to the gene level using the R package tximport v1.16.1 and differential abundance was analyzed using DESeq2 v1.28.1(Love et al., 2014; Soneson et al., 2015).

Genes that were potentially lncRNAs were identified based on ENSEMBL annotations (Howe et al., 2021). Reactome's "Interferon Signaling" pathway (R-HSA-913531) was used for the list of interferon stimulated genes (Fabregat et al., 2018). Heatmaps were generated with the ComplexHeatmap v2.4.3 R package implementing Ward's method for clustering (Gu et al., 2016; Ward, 1963). Data management was performed using base R and dplyr v1.0.2 (RCoreTeam, 2018; Wickham, 2017).

All sequencing data in this manuscript has been deposited with NCBI GEO and is available under accession number GSE184306.

High-throughput RNAi screening and analysis

Three, pooled, LNA-modified siRNAs per target were spotted into each well of a 384-well black tissue culture treated plate. siRNAs were acquired from a pre-designed library targeting 2200 lncRNAs across the human genome (Ambion). Briefly, 0.5 μL of HiPerfect diluted in 9.5 μL of Opti-MEM was added to each well using a ThermoFisher Scientific Matrix WellMate automated dispenser. Each plate containing the siRNA/HiPerfect mixture was then incubated at room temperature for 5-10 minutes. HBMEC (2500 cells/40 μL) were then added to each well using the WellMate and incubated for 3 days at 37°C, 5% CO_2. The final concentration of siRNA in each well was 30 nM. Following knockdown, CHIKV-mKate virus (MOI 0.05) was dispensed into each well followed by spinoculation at 2500 RPM for 1h at 4°C. Cells were then incubated at 37°C, 5% CO_2 for an additional 24h to allow infection to proceed. The cells were fixed with 4% formaldehyde/PBS for 10 min at room temperature. Finally, the cells were washed 3X with PBS, stained with

Hoechst 333432, and subjected to automated microscopy (ImageXpress, 10X objective). Four sites per well were acquired in two fluorescent channels.

For each parameter measured using the Cell Scoring module in MetaXpress (percent infection and total cell number) the data were first log transformed and the plate median and interquartile range (IQR) were calculated. Z scores were further calculated based on these values (($\log_{10}$(%infection) − $\log_{10}$(median)/(IQR × 0.74)). Any condition that resulted in Z<-2 for total cell number was removed from the infection datasets to avoid the potentially confounding effects of cytotoxicity on viral infection levels.

Cytokines and inhibitors

Human interferon β (IFNβ), tumor necrosis factor α (TNFα), and interleukin-1 β (IL-1β) were purchased from Peprotech, resuspended in phosphate buffered saline (PBS) and used at 10 ng/mL unless otherwise specified. AL8810 ($PGF_{2\alpha}$ inhibitor) was purchased from Santa Cruz Biotechnologies. SP600125 (JNK inhibitor), PD98059 (MEK1/2 inhibitor), and Ruxolitinib (JAK/STAT inhibitor) were purchased from Invivogen. AL8810, SP600125, and PD98095 were reconstituted per the manufacturer's instructions, used at the indicated concentrations, and were added to cells at the same time as viral inoculation. Ruxolitinib was also reconstituted per the manufacturer's instructions and used at the specified concentrations, but cells were instead pre-treated for 2h prior to infection. Ionomycin was purchased from Sigma, reconstituted in PBS, and used at the specified concentrations and time points. Mock and untreated controls were "stimulated" with the appropriate vehicle only at the highest volume used for the given experiment and reagent concentration.

RNA Interference

All knockdowns were performed using the Qiagen HiPerfect Fast-Forward protocol. For viral RNA and titer quantification, 10 μL of HiPerfect and 1.5 μL of 20 μM stock siRNA were diluted in 120 μL of Opti-MEM. These contents were vortexed for 5s and incubated at room temperature for 5-10 minutes. During incubation, $5x10^4$ cells were plated per well in a 12-well tissue culture-treated plate and complete HBMEC media was added to a volume of 875 μL. 125 μL of siRNA transfection mix was then added dropwise into each appropriate well. The final concentration of siRNA equated to 30 nM. Cells were then incubated at 37°C, 5% CO_2 for 72h followed by subsequent downstream treatments and infections. For viral breadth studies measured by immunofluorescence, a 384-well format was used. Briefly, 1.5 μL of 1 μM siRNA stock was spotted into each well in triplicate for each condition. 0.5 μL of HiPerfect was diluted in 9.5 μL of Opti-MEM per well, added to each well, and incubated at room temperature for 5-10 minutes. $2.5x10^3$ cells suspended in 40 μL of complete HBMEC media were then added to each well and incubated at 37°C, 5% CO_2 for 72h at which point downstream treatment and infections were performed.

Transfection and transduction

HBMEC were transfected using X-treme Gene 9 following the manufacturer's instructions. Cells were plated at a density of $1x10^5$ cells per well of a 6-well plate the day prior to transfection. 1 μg of plasmid was introduced at a 1:2 ratio with X-treme Gene 9 and incubated at 37°C, 5% CO_2 for 48h before further processing.

To produce lentivirus, HEK293T cells were simultaneously transfected with 1 μg lentiviral plasmid containing the cDNA of interest, 0.7 μg CMV-VSV-g (Addgene) and 1 μg of psPAX2 (Addgene) in a 12-well format using Lipofectamine 2000 per the manufacturer's protocol. Following a 24h incubation at 37°C, 5% CO_2, the media was replaced with 750 μL of fresh media followed by an additional 24h incubation. The supernatants were then collected and filtered through a 0.45 μm syringe filter and stored at -80°C. To transduce HBMEC, $5x10^4$ cells were plated in a 6-well plate in 2 mL complete media containing 100 μL viral supernatant and 10 μg/mL polybrene. Transduction was allowed to proceed for 48h followed by antibiotic selection and other downstream applications.

Immunofluorescence and microscopy

Cells were fixed in 4% formaldehyde/PBS for 10 minutes at room temperature (covered if fluorescently tagged viruses were used). Cells were then washed 3X in PBS and incubated in 0.5% Triton-X100/PBS (PBST) for 10 min at room temperature to permeabilize cell membranes. Cells were then blocked in 2% bovine serum albumin (BSA)/PBST for 30 min at room temperature followed by overnight incubation at 4°C in primary antibody diluted in 2% BSA/PBST. Cells were washed 3X with PBST followed by a 1h room temperature incubation in fluorescently conjugated secondary antibody diluted in 2% BSA/PBST. Cells were washed 3X in PBST and stored in PBS. Viral protein quantification (for lncRNA screens, viral breadth, and viral phenotyping in *ALPHA* knockdown, knockout, and overexpression studies) were performed using a Molecular Devices automated imager and analyzed with MetaXpress (Mulitwavelength Cell Scoring Module). Negative-strand quantification (measured by J2 staining) was imaged using a Leica DM5500 Q confocal microscope and quantified using ImageJ.

Nuclear/Cytoplasmic Fractionation

HBMEC ($5x10^5$) were trypsinized, collected via centrifugation, and resuspended in 200 μL of cytoplasmic lysis buffer (CLB; 30 mM HEPES pH 7.4, 2mM MgOAC, 0.1% NP-40). Lysates were then incubated on ice for 10 minutes and pipetted up and down gently every 2-3 minutes to promote lysis. The lysate was then centrifuged at 2300 RPM for 20 minutes at 4°C. The supernatant was removed, placed in a fresh 1.5 mL tube and kept on ice (cytoplasmic fraction). The nuclear pellet was then washed 3X with CLB (nuclei were centrifuged at 2300 RPM for 5 min between each wash). Nuclei were subsequently lysed in 200 μL nuclear lysis buffer

(NLB; CLB + 150 mM KOAc) and incubated on ice for 10 minutes, vortexing every 2-3 minutes to promote lysis. Both the cytoplasmic and nuclear lysates were sonicated 2X, 30s on and 30 off for 3 min (equating to roughly 1000 J of exposure). Lysates were then cleared at 10,000 RPM for 10 minutes at 4°C. Supernatants were removed, placed in 1.5 mL tubes, and 1 mL TRIzol was added for downstream RNA isolation. Primers for *GAPDH* and *MALAT1* were used as controls for the quality of the cytoplasmic and nuclear fractionations respectively. The relative enrichment of the RNA targets was quantified as a percentage of the total amplification of the combined nuclear and cytoplasmic values.

Viral entry, dsRNA quantification, viral spread, and anti-genome quantification

Both control and *ALPHA*-depleted cells were infected with CHIKV, MOI 20 in the presence of 10 μg/mL cycloheximide (CHX) for 4h. Cells were then incubated in 0.25% trypsin-EDTA for 7 min at 37°C, 5% CO_2 to remove bound virions that had not yet entered. Trypsin was neutralized 1:1 with complete media, cells were collected by centrifugation, and lysed in 1 mL TRIzol for downstream RNA isolation. To measure dsRNA production, control and *ALPHA*-depleted cells were plated on glass coverslips in a 24-well plate and infected with CHIKV, MOI 20 for 8h. Following infection, the cells were fixed with 4% formaldehyde for downstream immunofluorescence staining using J2 antibody. The coverslips were mounted onto glass slides using Vectashield (Vector Laboratories) prior to imaging. Viral spread was assayed by infecting control and *ALPHA*-depleted cells for 4h with CHIKV, MOI 0.05 followed by the addition of 20 mM NH_4Cl. Cells were lysed in TRIzol 20 hpi for downstream RNA isolation. Anti-genome quantification was performed as previously described (Meertens et al., 2019). Briefly, control and *ALPHA*-depleted HBMEC were infected for 8h at MOI 0.5. The cells were lysed in TRIzol and RNA was extracted as described below. Strand-specific reverse transcription was performed using a primer complementary to anti-genome at a final concentration of 100 nM following the manufacturer's protocol. The cDNA was diluted 1:10 prior to qPCR with anti-genome-specific primers. A gBlock encoding the 133 bp amplicon produced from these primers was synthesized by IDT and used to generate a standard curve ranging from $1x10^8$ to 10 DNA copies. Anti-genome copies were calculated based off of this standard curve.

CRISPR knockout generation

CRISPR reagents were generated as previously described (Sanjana et al., 2014; Shalem et al., 2014). Briefly, guide RNAs (gRNAs) flanking the 5' and 3' ends of the ALPHA locus (ENSG00000227075) were designed using the CRISPOR design algorithm. These gRNAs were cloned into lentiCRISPRv2 and lentivirus was generated as described above. HBMEC were transduced and selected using 1 μg/mL puromycin. Single cell clonal populations were genotyped and *ALPHA* levels quantified. Control cells were generated in an identical manner using two predefined, non-targeting gRNAs (Kearns et al., 2014; Mimee et al., 2015).

Stable ectopic expression cell line generation

pcDNA3.1-*ALPHA* (empty pcDNA3.1 was used to generate control cells) or pmCherry-N1-IFNb were transfected into HBMEC as described above and selected for 7 days with 1.5 mg/mL of G418. pcDNA3.1-*ALPHA* was synthesized by Genscript and pmCherry-N1-IFNb was a gift from Drs. Yueh-Ming Loo and Michael Gale (University of Washington). For *ALPHA* overexpressing clones, *ALPHA* levels were quantified by qPCR to confirm overexpression. For IFN-mCherry reporter HBMEC, cells were stimulated with SeV (100 HAU/mL) for 24h and imaged by immunofluorescence to confirm positive clones.

RNA isolation and quantitative reverse transcription PCR

Samples were lysed in TRIzol and RNA was extracted using the RNA Clean and Concentrator Kit (Zymogen) with on-column DNase I treatment per the manufacturer's instructions. Complementary DNA (cDNA) was generated using moloney murine leukemia virus (M-MLV) reverse transcriptase (Ambion) per the manufacturer's protocol. Quantitative PCR (qPCR) was performed in technical triplicate using 2X Power SYBR green/Rox qPCR Master Mix (ThermoScientific) and analyzed using relative Ct values. *GAPDH* was used as a normalization control for all experiments unless otherwise specified.

Polysome fractionation

HBMEC were grown to ~90% confluence in two 15 cm^2 tissue-culture treated plates. The media was removed, cells were washed 1X with PBS and fresh media containing 100 μg/mL cycloheximide (CHX) was added to the cells and allowed to incubate for 7 min at 37°C. The media was then removed and cells were collected and pelleted at 1200 RPM for 5 min. Cell pellets were washed 2X with PBS containing 100 μg/mL CHX and lysed in 250 μL Polysome Lysis Buffer (PLB; 100 mM KCl, 5 mM $MgCl_2$, 10 mM Hepes pH 7.4, and 0.5% NP-40) containing 100 μg/mL CHX, SUPERase-In (1 μL/1 mL PLB), and 1X protease inhibitor. Lysates were incubated on ice for 20 min (without vortexing). During the lysate incubation, a 10-50% sucrose gradient was prepared using a Seton Gradient Maker in a 10 mL ultracentrifuge tube. Following incubation, the lysates were then cleared at 13,200 RPM for 3 min at 4°C. Cleared lysate was then loaded on top of the prepared sucrose gradient and balanced to the hundredth decimal place. The sample was then spun using a SW-40i rotor at 35,000 RPM for 2.5 hours at 4°C. Fractions were then collected into 1.5 mL tubes using a Biocomp Piston Gradient Fractionator per the manufacturer's protocol. Each fraction was additionally split into 250 μL volumes, lysed in TRIzol, and stored at -80°C for further RNA extraction.

UV-inactivation of virus:

Virus (300 μL) was placed in a 60 mm^2 tissue culture dish and rotated to spread and maximize the surface area for exposure. With the lid removed, virus was exposed to 1200 μJ x 100 of 254 nm UV light using a Stratalinker 2400. This exposure was repeated 5X, rotating the plate between each UV treatment. The UV-inactivated virus was placed in a fresh 1.5 mL tube and kept on ice until further use. Equivalent volumes of either WT or UV-inactivated virus were used based on the calculated WT MOI.

Viral Titer Quantification

To measure viral titers produced in control or *ALPHA*-depleted HBMEC, cells were infected for 6h at the indicated MOIs. The media was then removed and the cells were washed 3X with PBS. Fresh, complete HBMEC media was added to each well and the infection was allowed to continue for 24h from that point. Supernatants were then used for $TCID_{50}$ assays on either BHK-21 or Vero cells. The day before inoculation, $1.5x10^4$ cells were plated in quadruplicate in a 96-well black tissue-culture treated plate. Ten-fold serial dilutions of viral supernatants were prepared in Opti-MEM in 10 μL volumes and added to the appropriate wells. The cells were then incubated for 24h at 37°C, 5% CO_2 followed by fixation with 4% formaldehyde. Infection was quantified by immunofluorescence and automated imaging as described. $TCID_{50}$s were calculated using the Reed-Muench Method (Reed and Muench, 1938).

RNA-RNA Interactions Probe Generation

Templates for *in vitro* transcription were generated by PCR amplification from either uninfected HBMEC cDNA (*GAPDH*) or cDNA generated from purified viral RNA (CHIKV and SINV genomic RNA) with the addition of T7 (5') and/or SP6 (3') promoter sequences to the amplicon ends. PCR was performed using Phusion DNA Polymerase per the manufacturer's protocol and products were purified using the Qiagen PCR Purification Kit. Probe RNA was synthesized using either a T7 (sense RNA) or SP6 (antisense RNA) MEGAscript Kit (ThermoFisher Scientific) following the manufacturer's instructions and purified by lithium chloride extraction. The probes were then biotinylated using the Pierce™ RNA 3' End Biotinylation Kit (ThermoFisher Scientific) following the manufacturer's instructions (incorporating 50 pmol of RNA per reaction).

In cellulo RNA-RNA Interactions

HBMEC ($1x10^7$ cells, either HBMEC or *ALPHA*-overexpressing HBMEC) were either uninfected or infected with CHIKV or SINV at a MOI 2 for 20h. Following infection, the media was removed and cells were trypsinized and centrifuged at 1200 RPM for 5 min to pellet. The cell pellets were washed 1X with PBS and centrifuged again at 1200 RPM for 5 min. Each pellet was then resuspended in 1% glutaraldehyde/PBS and incubated with orbital rotation for 10 min at room temperature. The glutaraldehyde crosslinking solution was subsequently quenched with $1/10^{th}$ (1 mL) volume of 1 M glycine and incubated at room temperature with orbital rotation for 5 min. The cells were then pelleted at 2000 RCF for 5 min at room temperature and washed 1X with PBS. Cells were then pelleted at 2000 RCF for 5 min at 4°C and resuspended in 1 mL of PBS. The cell suspension was transferred to a 1.5 mL tube and centrifuged at 2000 RCF for 5 min at room temperature. The supernatants were removed, the pellets were flash frozen on dry ice, and stored at -80°C until further processing.

Frozen cell pellets were thawed quickly at room temperature followed by a pulse spin to collect and remove any remaining supernatant. The pellets were then lysed in 300 μL Lysis Buffer (LB; 50 mM Tris-Cl pH 7.0, 10 mM EDTA, 1% SDS) containing protease inhibitor (Roche Applied Science), PMSF, and SUPERase-In (Ambion, stock treated as 200X) and immediately subjected to sonication. The lysates were then cleared at 10,000 RPM for 10 min, placed in fresh 1.5 mL tubes, and kept on ice. 20 μL of lysate (6.7%) was removed as input control and stored at -80°C. The remaining lysate was split into 1.5 mL tubes containing 250 μL Hybridization Buffer (HB; 750 mM NaCl, 50 mM Tris-Cl, 1 mM EDTA, 1% SDS, 15% formamide) with added protease inhibitor, PMSF, and SUPERase-In, and 12.5 pmol of the biotinylated, 500mer, antisense oligonucleotide probe designed to target either a control transcript (*GAPDH*), CHIKV genomic RNA, or SINV genomic RNA. The probes were hybridized at 37°C with rotation for 16-20h. Streptavidin-conjugated magnetic beads (50 μL/sample) were washed 3X in unsupplemented LB and resuspended in the original volume of LB containing protease inhibitor, PMSF, and SUPERase-In. Washed beads were then added to the lysate/hybridization solution and incubated for 1h at 37°C with rotation. Samples were placed on a DynaMag-2 magnet to collect beads. Supernatants were removed and discarded. Beads were resuspended in Wash Buffer (WB; 2X SSC, 0.5% SDS) containing PMSF and placed in fresh 1.5 mL tubes. The samples were then incubated at 37°C for 4 min with rotation. Samples were placed on a DynaMag-2 magnet to collect beads and then resuspended in WB containing PMSF. These wash steps were performed 5X in total. Following the final wash, the beads were pulse spun and placed back on the magnet to remove residual WB. The beads were then resuspended in 95 μL Proteinase K Buffer (PKB; 100 mM NaCl, 10 mM Tris-Cl, 1 mM EDTA, 0.5% SDS). Input samples were concordantly thawed at room temperature and 75 μL of PKB was added to each. 5 μL of Proteinase K (final concentration: 5 μg/mL) was added to each sample and incubated at 50°C with 250 RPM orbital rotation for 45 min. The samples were then heated to 95°C for 10 min and immediately placed on ice. Each sample was then resuspended in TRIzol and stored at -80°C until further processing.

In vitro RNA-RNA Interactions

For Figures 5B–5D, 200 ng of each biotinylated probe was mixed with 200 ng unbiotinylated CHIKV replicon RNA in 300 μL Binding Buffer (20 mM Tris-HCL ph 7.4, 1 M NaCl, 2 mM EDTA, 0.1% SDS, (Gorbea et al., 2017)) and incubated for 2h at room temperature with rotation. For Figures 5E–5H, 300 ng of biotinylated, full-length CHIKV replicon RNA was combined with 30 ng of

unbiotinylated *ALPHA*, representing a ~1:1 molar ratio. The quantities of biotinylated nsp1-4 used were calculated to equate to 300 ng of the full-length replicon by molar ratios. Streptavidin-conjugated beads (15 μL per sample) were washed 3X with Binding Buffer prior to being added to each sample. The beads were then incubated with the samples at room temperature for 30 min with rotation. Samples were then placed on a Dynmag-2 magnet to collect beads and the supernatants were discarded. The beads were washed 3X with Binding Buffer, resuspended in 500 μL of TRIzol and stored at -80 until ready for RNA extraction, cDNA synthesis, and qPCR.

RNA Proximity Ligation Assay (RNA-PLA)

HBMEC (2 x 10^4 cells) were plated on 12 mm^2 round coverslips in a 24-well plate the day prior to infection. Cells were infected with CHIKV, MOI 5 for 24h and fixed using 4% formaldehyde/PBS for 10 min at room temperature. Cells were then permeabilized using 0.2% Triton-X 100/PBS for 10 min at room temperature and blocked for 1h in PLA Blocking Buffer (10 mM Tris-Acetate, 10 mM magnesium acetate, 50 mM potassium acetate, 250 mM NaCl, 0.25 μg/μL BSA, 0.05% Tween-20) at 37°C. Coverslips were then incubated overnight with 200 nM PLA probe solution (100 nM each of priming and non-priming probe diluted in PLA Blocking Buffer) at 37°C in a sealed humidity chamber. The specific probe pairings are as follows: GAPDH-Priming + CHIKV-Non-Priming, CHIKV(50 nt downstream)-Priming + CHIKV-Non-Priming, ALPHA-Priming + CHIKV-Non-Priming, and GAPDH-Priming + ALPHA-Non-Priming. The same CHIKV-Non-Priming probe was used in each condition where CHIKV RNA was targeted. Cells were washed 3X with PBS, 5 min each at room temperature. Ligation mix was prepared immediately before placement on coverslips containing 125 nM PLA connector, 125 nM PLA linker, and 1 μL T4 ligase in 1X T4 ligation buffer. Ligation was carried out at 37°C for 30 min followed by 3X washes with PBS, 5 min each at room temperature. Rolling circle amplification and amplicon detection was performed using 10 nM PLA amplicon probe (Cy5-conjugated), 100 μM dNTPS, 10 μg/mL BSA, and 1 μL phi29 polymerase in 1X phi29 reaction buffer at 37°C for 1h, 40 min. Cells were then washed 1X in PBS containing Hoechst solution for 10 min at room temperature followed by 2X washes in PBS. Coverslips were mounted using Vectashield and imaged using a Leica DM5500 Q confocal microscope. Puncta from 40-60 cells per condition were counted in each replicate using ImageJ.

All PLA oligonucleotide sequences were designed as previously described containing a three-part structure: i.) a 40-50 nucleotide sequence complementary to a target RNA of interest ii.) a 17-20 nucleotide poly(A) linker and iii.) an assay-specific, non-targeting PLA sequence (Fredriksson et al., 2002; Söderberg et al., 2006; Zhang et al., 2016). The complementary region was designed using the Stellaris Probe Designer tool (https://www.biosearchtech.com/support/tools/design-software/stellaris-probe-designer). The poly(A) linker and PLA sequences were then appended to the 3' end as is shown in the key resources table.

QUANTIFICATION AND STATISTICAL ANALYSIS

All statistics performed on fold change data were $\log_2$ transformed prior to analysis. Each dot represents an individual experiment. All analyses were performed as indicated using Prism or R.

Molecular Cell, Volume *82*

Supplemental information

The lncRNA *ALPHA* specifically targets chikungunya virus to control infection

Megha G. Basavappa, Max Ferretti, Mark Dittmar, Julian Stoute, Megan C. Sullivan, Kanupriya Whig, Hui Shen, Kathy Fange Liu, David C. Schultz, Daniel P. Beiting, Kristen W. Lynch, Jorge Henao-Mejia, and Sara Cherry

Molecular Cell, Volume *82*

Supplemental information

The lncRNA *ALPHA* specifically targets chikungunya virus to control infection

Megha G. Basavappa, Max Ferretti, Mark Dittmar, Julian Stoute, Megan Sullivan, Kanupriya Whig, Hui Shen, Kathy Fange Liu, David C. Schultz, Daniel Beiting, Kristen Lynch, Jorge Henao-Mejia, and Sara Cherry

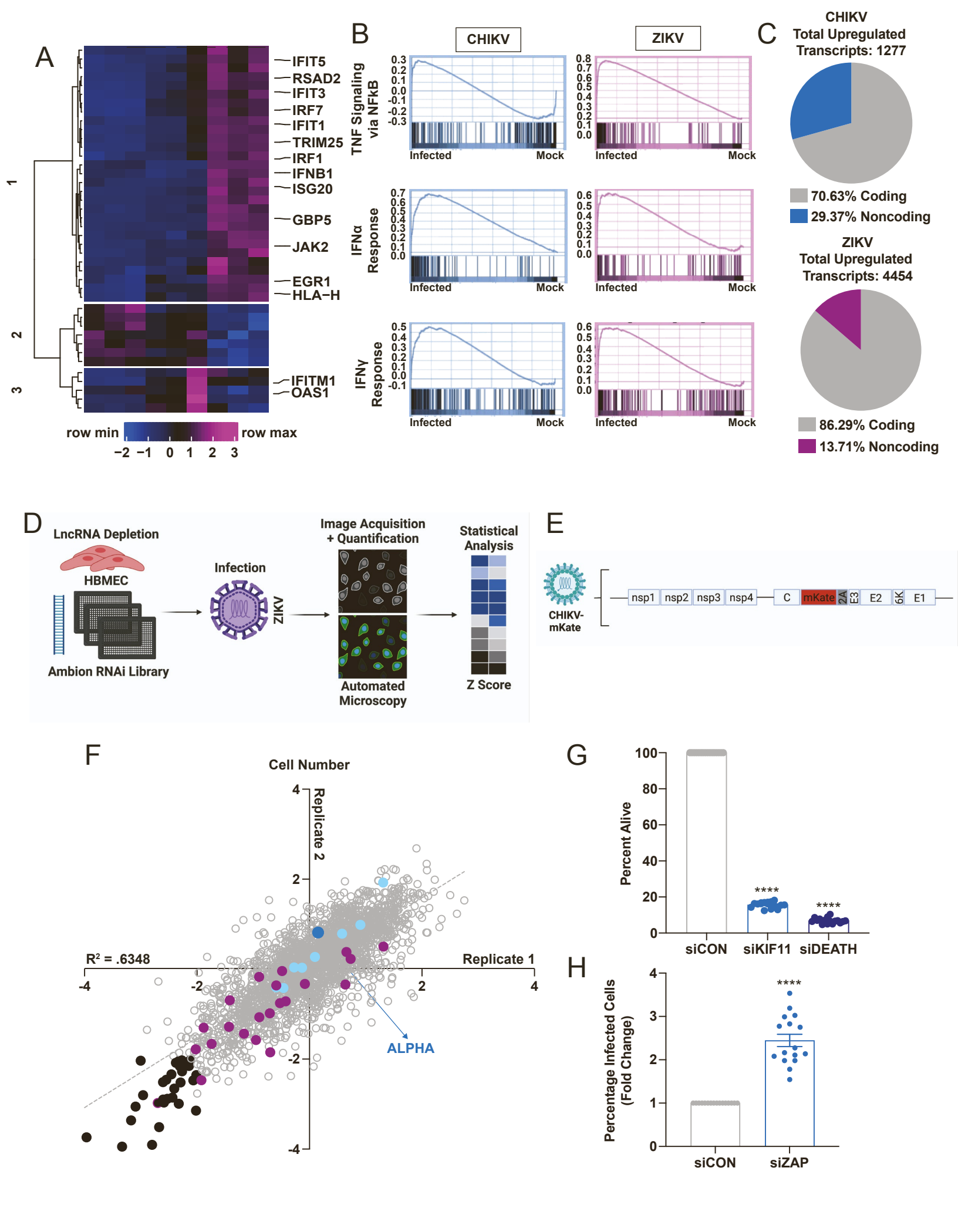
A
IFIT5
RSAD2
IFIT3
IRF7
IFIT1
TRIM25
IRF1
IFNB1
ISG20
GBP5
JAK2
EGR1
HLA−H
IFITM1
OAS1
1
2
3
row min
row max
−2 −1 0 1 2 3
B
CHIKV
ZIKV
TNF Signaling via NFkB
IFNα Response
IFNγ Response
Infected
Mock
C
CHIKV
Total Upregulated Transcripts: 1277
70.63% Coding
29.37% Noncoding
ZIKV
Total Upregulated Transcripts: 4454
86.29% Coding
13.71% Noncoding
D
LncRNA Depletion
HBMEC
Ambion RNAi Library
Infection
ZIKV
Image Acquisition + Quantification
Automated Microscopy
Statistical Analysis
Z Score
E
CHIKV-mKate
nsp1
nsp2
nsp3
nsp4
C
mKate
2A
E3
E2
6K
E1
F
Cell Number
Replicate 2
Replicate 1
R² = .6348
ALPHA
G
Percent Alive
siCON
siKIF11
siDEATH
****
H
Percentage Infected Cells (Fold Change)
siCON
siZAP
****

Figure S1, Related to Figure 1: High-throughput approaches reveal putative antiviral lncRNAs (A-C) HBMEC were uninfected or infected with CHIKV or ZIKV at MOI 5 for 24h in three independent experiments and subjected to total RNA-seq. Displayed are (A) Heat maps depicting IFN responsive gene expression with log_2 fold change greater than 1, read cutoff of 50, and adjusted p value of less than 0.05 in CHIKV and ZIKV-infected cells. (B) Gene set enrichment (GSEA) plots of enriched signatures induced by CHIKV or ZIKV in HBMEC. Y-axis represents enrichment score (ES). (C) Pie charts indicating the percentage of significantly upregulated transcripts which are coding vs. noncoding. Exact transcript numbers are shown. (D) Schematic describing the screen pipeline: a predesigned RNAi library targeting 2200 lncRNAs was transfected into HBMEC and knockdown was allowed to proceed for 3 days. The cells were then infected with CHIKV-mKate at MOI 0.05 for 24h, fixed and immunostained for nuclei (Hoechst). Images were acquired using automated microscopy and the percentage of cells infected was quantified. The screen was performed in duplicate and statistically analyzed using Z scores. (E) The structure of the CHIKV-mKate virus used in the screen is shown. (F) Cell number was measured using Hoechst staining and automated microscopy and Z scores were calculated. Data points with Z<-2 are highlighted in black and were removed from percent infection data shown in Figure 1B. The antiviral and proviral candidates from Figure 1B are highlighted in light blue and purple respectively. *ALPHA* is highlighted in dark blue. (G) siRNAs targeting the pro-mitotic *KIF11* and anti-apoptotic genes (siDEATH) were used as controls for RNAi efficiency within the screen. Cell number was measured by Hoechst staining and automated microscopy. (H) siRNAs targeting *ZAP* were included as a positive control for an antiviral effect. Percent infection was measured by automated microscopy. Data are presented as fold change relative to siCON. n=2-3; RNA-seq data are displayed as log_2 fold change with $p<0.05$. ****$p<0.001$; error bars represent S.E.M.; n=2; Statistical analyses were performed using one-way ANOVA with Dunnett correction for multiple comparisons (G), Student's (unpaired, two-tailed) *t* test (H).

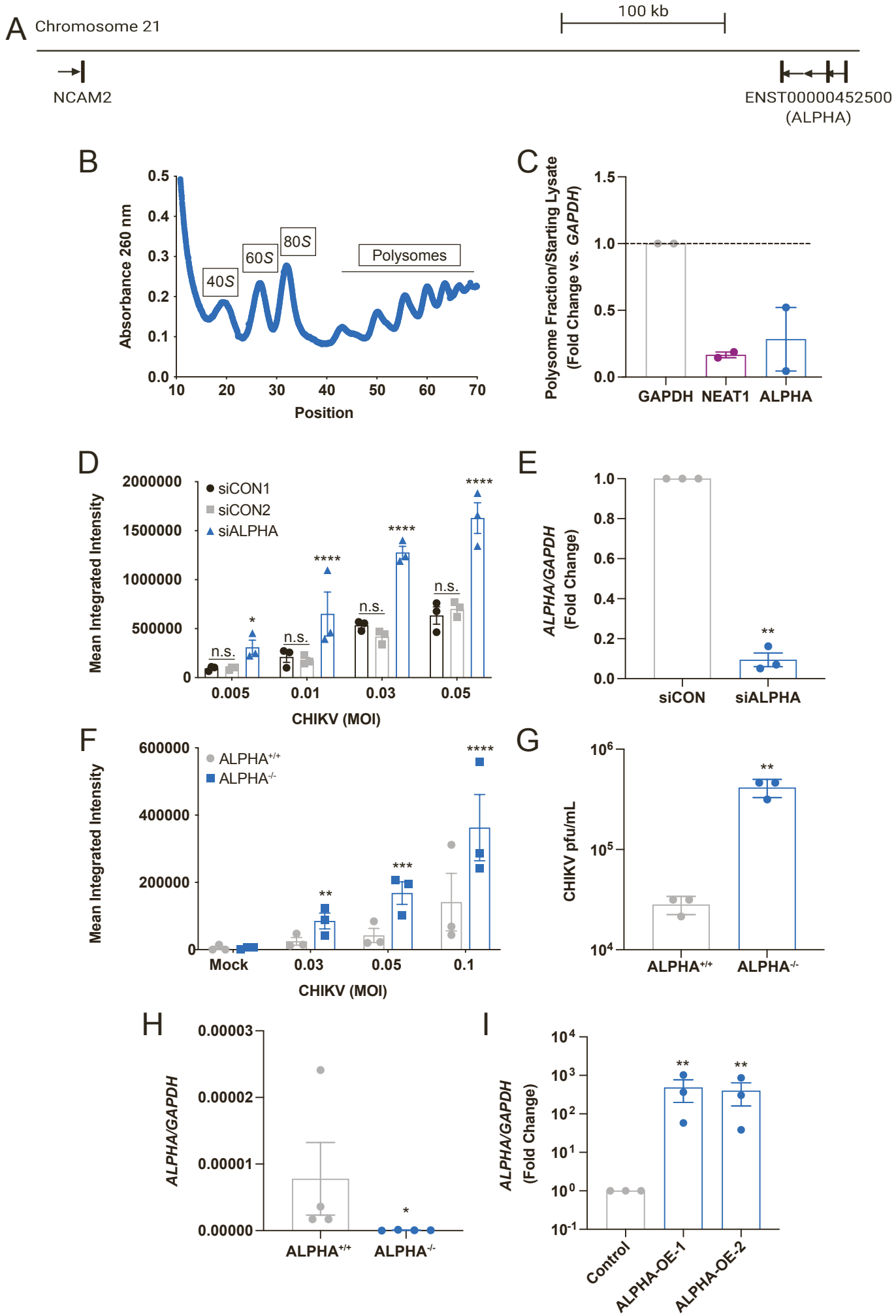
A
Chromosome 21
100 kb
NCAM2
ENST00000452500
(ALPHA)
B
Absorbance 260 nm
40S
60S
80S
Polysomes
Position
C
Polysome Fraction/Starting Lysate
(Fold Change vs. GAPDH)
GAPDH
NEAT1
ALPHA
D
Mean Integrated Intensity
siCON1
siCON2
siALPHA
n.s.
*
****
CHIKV (MOI)
E
ALPHA/GAPDH
(Fold Change)
siCON
siALPHA
F
Mean Integrated Intensity
ALPHA+/+
ALPHA-/-
Mock
CHIKV (MOI)
G
CHIKV pfu/mL
H
ALPHA/GAPDH
I
ALPHA/GAPDH
(Fold Change)
Control
ALPHA-OE-1
ALPHA-OE-2

Figure S2, Related to Figure 1: Characterization of *ALPHA* biology and function (A) The *ALPHA* locus is encoded in Chromosome 21 and is comprised of 3 exons spanning 42 kb transcribed in the antisense direction relative to the nearest coding gene. The most proximal coding gene is neural cell adhesion molecule (NCAM)2 which is ~500 kb away. (B) Polysome fractions were isolated from HBMEC using a sucrose gradient and collected using a Biocomp Piston Gradient Fractionator. The y-axis refers to A_{260} absorbance values and the x-axis refers to fraction position. (C) RNA was isolated from either unfractionated total lysate or polysome fractions (positions 45-70) and *GAPDH*, *NEAT1*, and *ALPHA* were quantified by qPCR. *GAPDH* was used a positive control for a translated mRNA and *NEAT1* was used as a negative control for an untranslated ncRNA. Data are displayed as enrichment relative to total lysate. (D) *ALPHA* was depleted in HBMEC using pooled siRNAs and infected with CHIKV-mKate at the indicated MOIs for 24h. CHIKV protein was measured using immunofluorescence and automated microscopy. (E) Quantification of *ALPHA* in RNAi-depleted HBMEC by qPCR. (F-G) $ALPHA^{+/+}$ and $ALPHA^{-/-}$ HBMEC were (F) infected with CHIKV-mKate at the indicated MOIs for 24h and viral protein was quantified by immunofluorescence and automated microscopy or (G) infected with CHIKV MOI 0.2 for 30h and titers were quantified by $TCID_{50}$. *ALPHA* levels in (H) $ALPHA^{+/+}$ and $ALPHA^{-/-}$ HBMEC and (I) control and *ALPHA*-overexpressing HBMEC as measured by qPCR. Data in (I) are represented as fold change vs. control cells. *GAPDH* was used as a loading control in all qPCR experiments unless otherwise specified. *p<0.05, **p<0.01, ***p<0.001, ****p<0.0001; error bars are S.E.M.; n=2-4 as indicated; Statistical analyses were performed using two-way ANOVA with Sidak correction for multiple comparisons (D, F), Student's (unpaired, two-tailed) *t* test (E, G, H), one-way ANOVA with Dunnet correction for multiple comparisons (I).

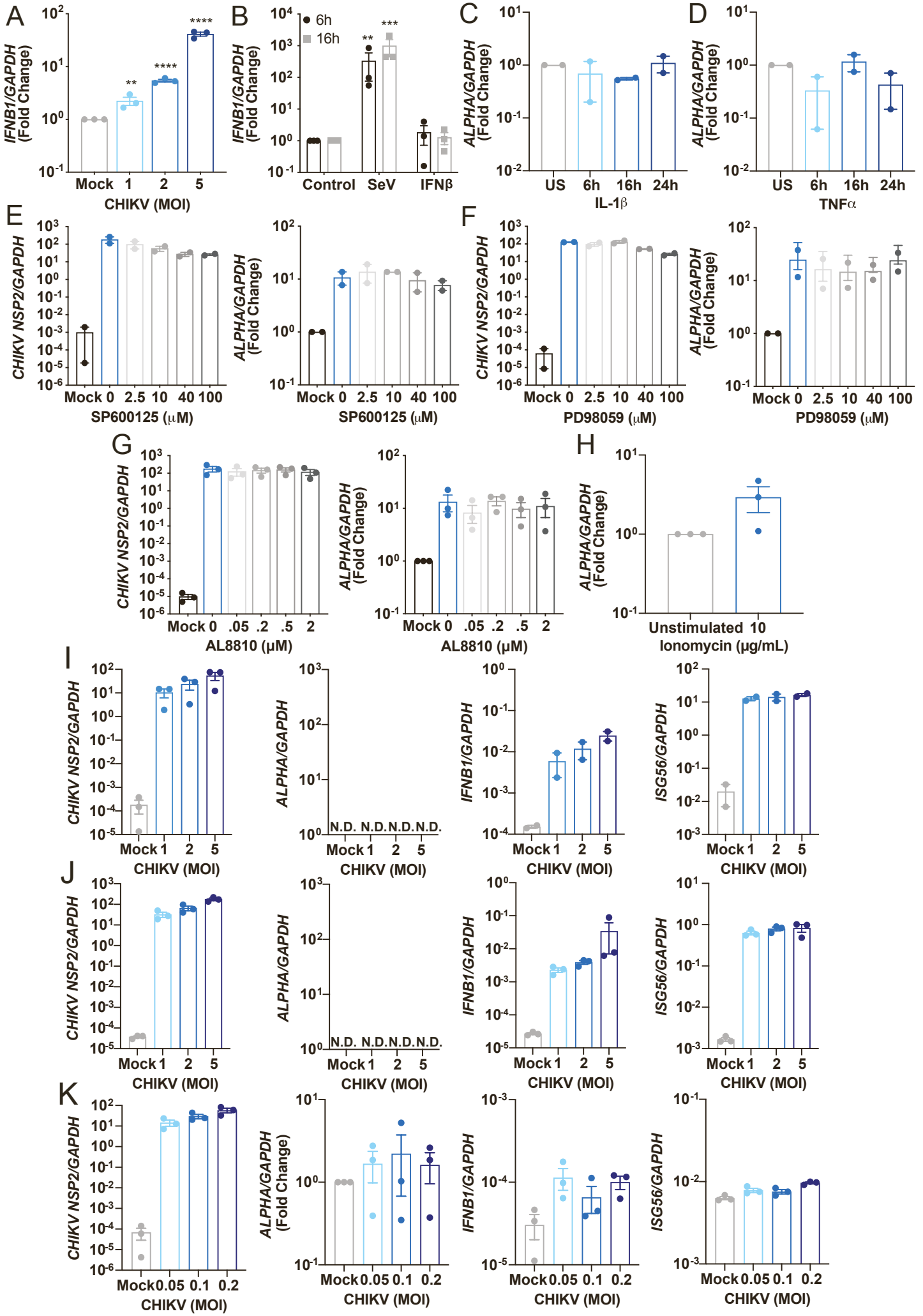
A
IFNB1/GAPDH (Fold Change)
Mock 1 2 5
CHIKV (MOI)
B
6h
16h
IFNB1/GAPDH (Fold Change)
Control SeV IFNβ
C
ALPHA/GAPDH (Fold Change)
US 6h 16h 24h
IL-1β
D
ALPHA/GAPDH (Fold Change)
US 6h 16h 24h
TNFα
E
CHIKV NSP2/GAPDH
Mock 0 2.5 10 40 100
SP600125 (μM)
ALPHA/GAPDH (Fold Change)
Mock 0 2.5 10 40 100
SP600125 (μM)
F
CHIKV NSP2/GAPDH
Mock 0 2.5 10 40 100
PD98059 (μM)
ALPHA/GAPDH (Fold Change)
Mock 0 2.5 10 40 100
PD98059 (μM)
G
CHIKV NSP2/GAPDH
Mock 0 .05 .2 .5 2
AL8810 (μM)
ALPHA/GAPDH (Fold Change)
Mock 0 .05 .2 .5 2
AL8810 (μM)
H
ALPHA/GAPDH (Fold Change)
Unstimulated 10
Ionomycin (μg/mL)
I
CHIKV NSP2/GAPDH
Mock 1 2 5
CHIKV (MOI)
ALPHA/GAPDH
N.D. N.D. N.D. N.D.
CHIKV (MOI)
IFNB1/GAPDH
CHIKV (MOI)
ISG56/GAPDH
CHIKV (MOI)
J
CHIKV NSP2/GAPDH
CHIKV (MOI)
ALPHA/GAPDH
N.D. N.D. N.D. N.D.
CHIKV (MOI)
IFNB1/GAPDH
CHIKV (MOI)
ISG56/GAPDH
CHIKV (MOI)
K
CHIKV NSP2/GAPDH
Mock 0.05 0.1 0.2
CHIKV (MOI)
ALPHA/GAPDH (Fold Change)
Mock 0.05 0.1 0.2
CHIKV (MOI)
IFNB1/GAPDH
Mock 0.05 0.1 0.2
CHIKV (MOI)
ISG56/GAPDH
Mock 0.05 0.1 0.2
CHIKV (MOI)

Figure S3, Related to Figure 2: CHIKV-induced *ALPHA* upregulation is independent of classical signaling pathways and is cell type-specific (A) HBMEC were infected with CHIKV for 24h at the indicated MOIs. *IFNB1* was measured by qPCR to assess activation of an innate immune response. Data are displayed as fold change vs. unstimulated cells. (B) HBMEC were treated with either Sendai virus (SeV, 100 HAU/mL) or recombinant IFNβ (10 ng/mL) for 6 or 16h and *IFNB1* was quantified by qPCR. Data are displayed as fold change vs. unstimulated cells. (C-D) HBMEC were stimulated with (C) IL-1β or (D) TNFα at 10 ng/mL for the indicated time points. *ALPHA* transcripts were measured by qPCR. Unstimulated cells are marked as US. (E-G) HBMEC were infected with CHIKV at MOI 5 for 24h and simultaneously treated with (E) SP600125 (JNK inhibitor) (F) PD98059 (MEK inhibitor) or (G) AL8810 ($PGF_{2\alpha}$ antagonist). CHIKV RNA and *ALPHA* were quantified in each of these experiments by qPCR. (H) Ionomycin (10 μg/mL) was used to stimulate Ca^{2+} signaling for 24h and *ALPHA* was quantified by qPCR. (I) Primary human peripheral blood monocytes, (J) A549 lung epithelial carcinoma cells, and (K) U2OS osteosarcoma cells were infected with CHIKV at the indicated MOIs for 24h. CHIKV RNA, *ALPHA*, *IFNB1*, and *ISG56* were quantified by qPCR. *ALPHA* expression is displayed as fold change relative to uninfected (mock) cells. *GAPDH* was used as a loading control in all experiments. **p<0.01, ***p<0.001, ****p<0.0001; error bars are S.E.M.; n=2-3 as indicated; Statistical analyses were performed using one-way ANOVA with Dunnett correction for multiple comparisons (A, G), two-way ANOVA with Tukey correction for multiple comparisons (B), Student's (unpaired, two-tailed) *t* test (H).

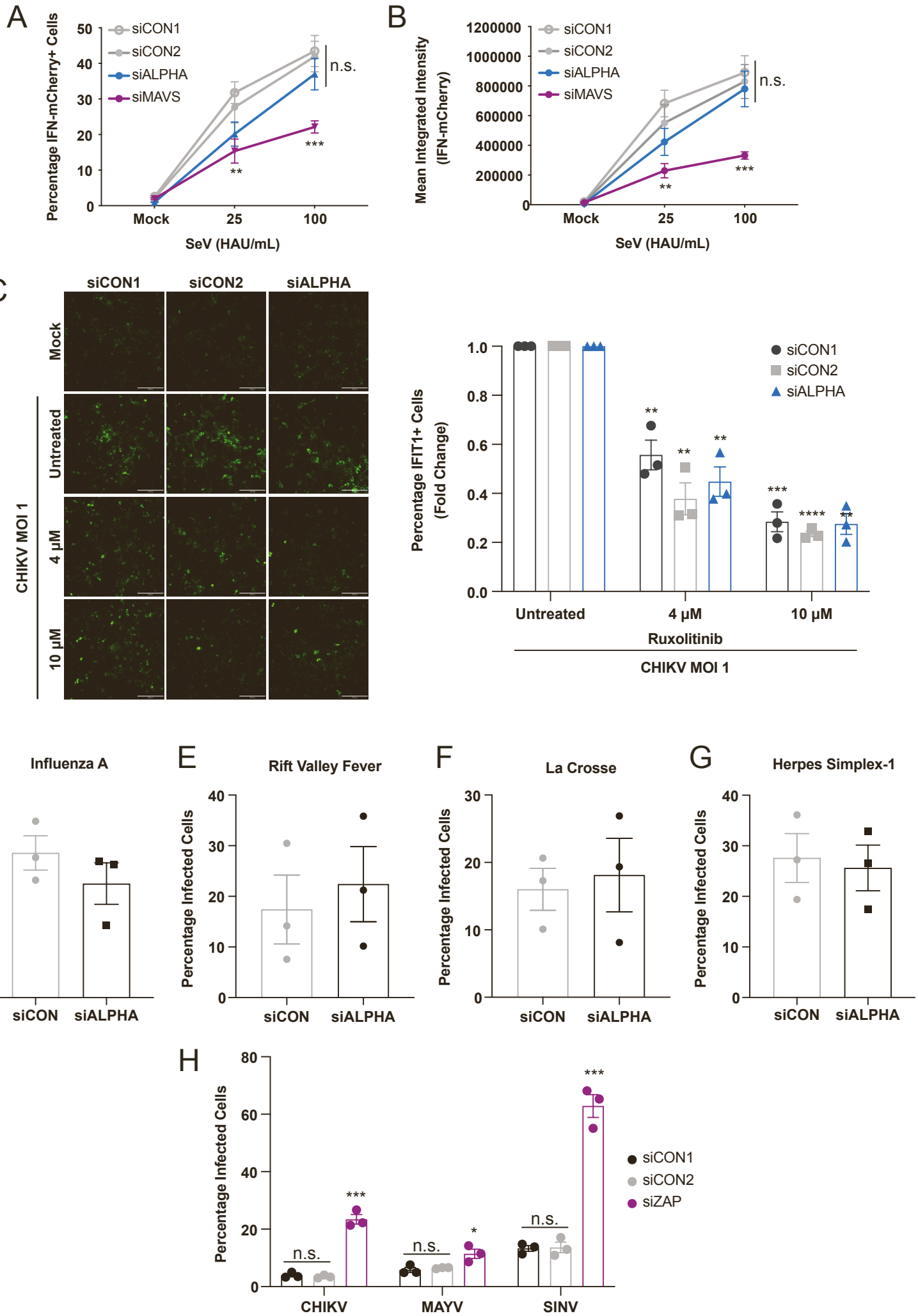
A
Percentage IFN-mCherry+ Cells
siCON1
siCON2
siALPHA
siMAVS
n.s.
**
***
Mock
25
100
SeV (HAU/mL)
B
Mean Integrated Intensity (IFN-mCherry)
C
siCON1
siCON2
siALPHA
Mock
Untreated
4 μM
10 μM
CHIKV MOI 1
Percentage IFIT1+ Cells (Fold Change)
Untreated
4 μM
10 μM
Ruxolitinib
CHIKV MOI 1
D
Influenza A
E
Rift Valley Fever
F
La Crosse
G
Herpes Simplex-1
Percentage Infected Cells
siCON
siALPHA
H
siZAP
CHIKV
MAYV
SINV
*

Figure S4, Related to Figures 2 and 3: *ALPHA* activity is IFN-independent and virus-specific

(A-B) HBMEC stably expressing an IFN-mCherry reporter were stimulated with SeV for 24h at the indicated concentrations following transfection with non-targeting siRNAs or siRNAs against *ALPHA* or *MAVS*. (A) Percent infection and (B) MFI were quantified by immunofluorescence and automated microscopy. (C) HBMEC were pre-treated for 2h with ruxolitinib at the indicated concentrations followed by spin infection with CHIKV at MOI 1 for 24h. Representative images are shown (left). The percentage of IFIT1+ cells was quantified by immunofluorescence and automated microscopy (right). Data are displayed as fold change relative to the corresponding untreated control. Scale bars represent 200 μm. (D-G) Control or *ALPHA*-depleted HBMEC were infected with (D) Influenza A (IAV, MOI 0.02), (E) Rift Valley Fever Virus (RVFV, MOI 0.01), (F) La Crosse Virus (LACV, MOI 0.01), or (G) Herpes Simplex Virus 1-GFP (HSV-1-GFP, MOI 0.005). The percentage of infected cells was quantified by immunofluorescence and automated microscopy. (H) Control or *ZAP*-depleted HBMEC were infected with CHIKV (MOI 0.03), MAYV (MOI 0.1), or SINV (MOI 0.1) for 24h. The percentage of infected cells was quantified by immunofluorescence and automated microscopy. *p<0.05, **p<0.01, ***p<0.001, ****p<0.0001; error bars are S.E.M.; n=3; Statistical analyses were performed using two-way ANOVA with Tukey correction for multiple comparisons. Significance shown is relative to siCON1 (A, B), Student's (unpaired, two-tailed) *t* test with Holm-Sidak correction for multiple comparisons (C, H), Student's (unpaired, two-tailed) *t* test (D-G).

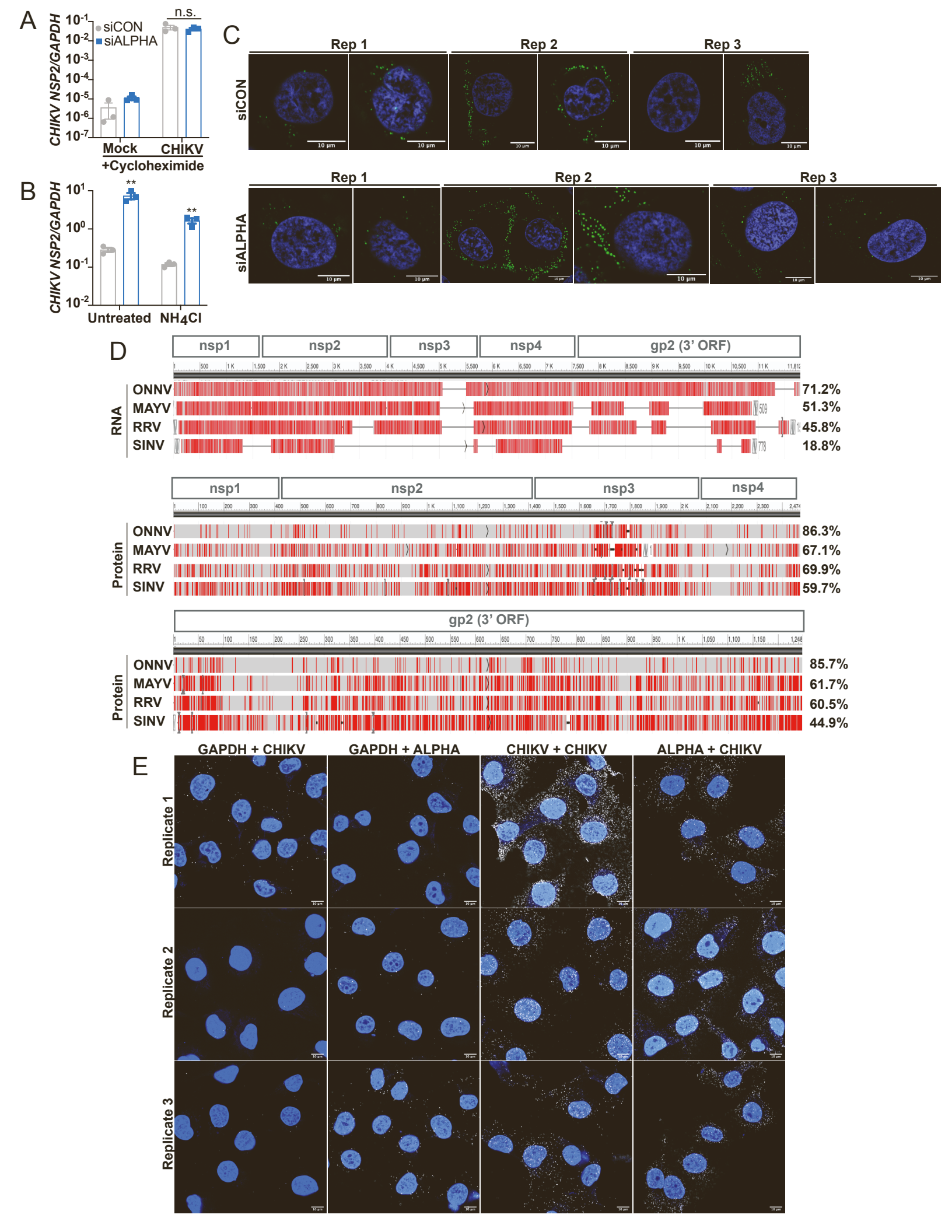
A
CHIKV NSP2/GAPDH
siCON
siALPHA
n.s.
Mock
CHIKV
+Cycloheximide
B
CHIKV NSP2/GAPDH
**
**
Untreated
NH4Cl
C
Rep 1
Rep 2
Rep 3
siCON
siALPHA
10 µm
D
nsp1
nsp2
nsp3
nsp4
gp2 (3' ORF)
RNA
ONNV
MAYV
RRV
SINV
71.2%
51.3%
45.8%
18.8%
Protein
86.3%
67.1%
69.9%
59.7%
85.7%
61.7%
60.5%
44.9%
E
GAPDH + CHIKV
GAPDH + ALPHA
CHIKV + CHIKV
ALPHA + CHIKV
Replicate 1
Replicate 2
Replicate 3

Figure S5, Related to Figure 4: *ALPHA* does not regulate CHIKV entry or spread and interacts with CHIKV RNA in the cytoplasm (A) Control and *ALPHA*-depleted HBMEC were infected with CHIKV at MOI 20 for 4h in the presence of cycloheximide (10 μg/mL), extracellular virions were removed by trypsinization and intracellular CHIKV RNA was quantified by qPCR. (B) Control and *ALPHA*-depleted HBMEC were infected with CHIKV at MOI 0.05 for 4h followed by addition of either vehicle control or ammonium chloride (NH_4Cl) for 24h. Viral RNA levels were quantified by qPCR. *GAPDH* was used as a loading control for (A) and (B). (C) Additional representative images for each independent experiment in Figure 4A are shown. Scale bars represent 10 μm. (D) RNA and protein sequence alignments between related alphaviruses CHIKV (Ross), ONNV (SG650), MAYV (BeH407), RRV (T48), and SINV (Girdwood) generated using megaBLAST. The dark gray line at the top represents the CHIKV Ross reference sequence. Light gray rectangles represent regions of detected homology. Red lines demarcate nucleotides or amino acids which differ from CHIKV Ross. Thin black horizontal lines represent regions where there is no detectable homology. Percent identity compared to CHIKV Ross is indicated on the left. (E) HBMEC were infected with CHIKV at MOI 5 for 24h and subjected to PLA. Additional images corresponding to main Figure 4D-E from all three replicates are shown. Scale bars represent 10 μm. **$p<0.01$; error bars are S.E.M.; n=3; Statistical analyses were performed using two-way ANOVA with Sidak correction for multiple comparisons (A), Student's (unpaired, two-tailed) *t* test with Holm-Sidak correction for multiple comparisons (B).

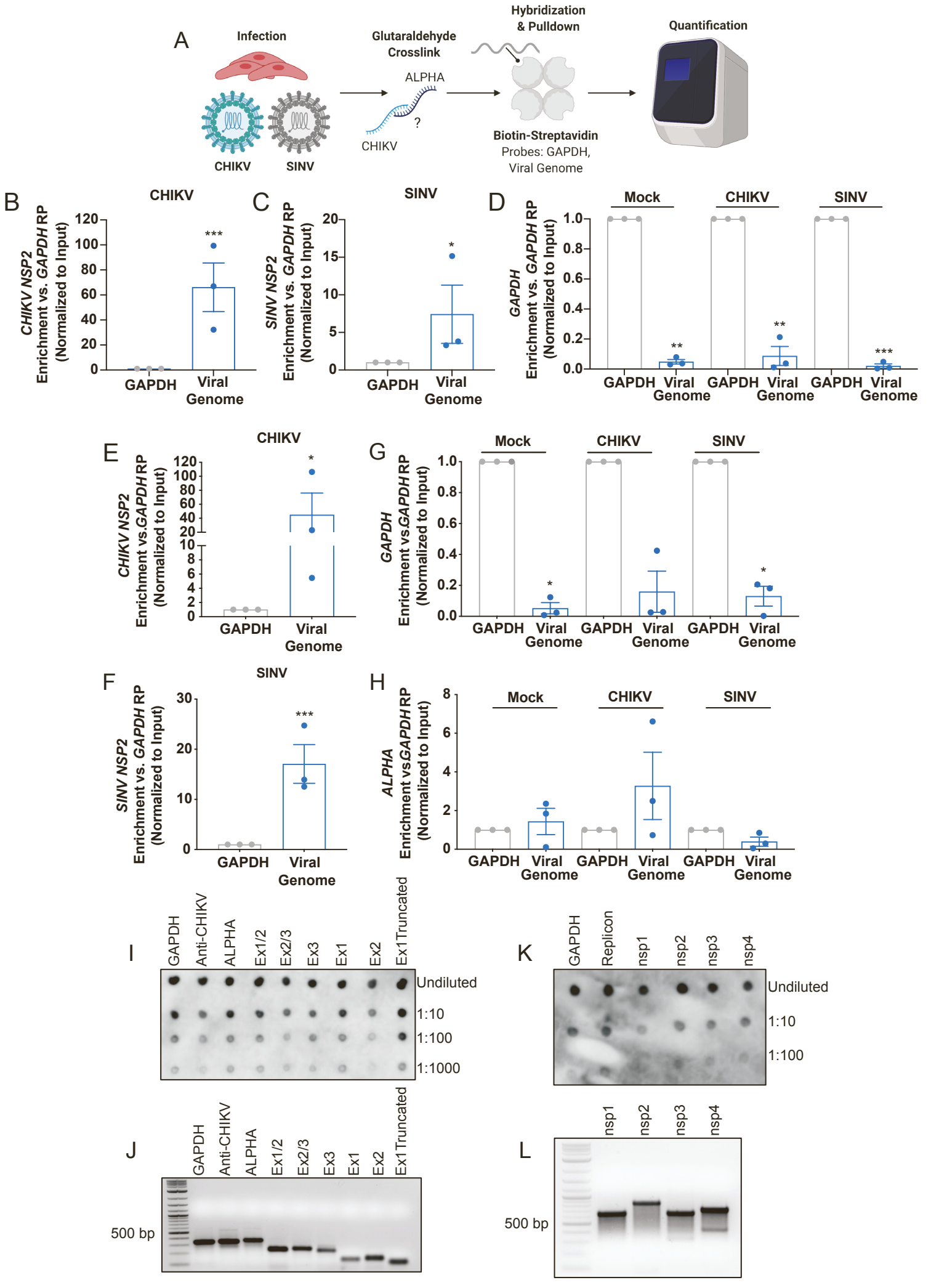
A
Infection
CHIKV
SINV
Glutaraldehyde Crosslink
ALPHA
?
CHIKV
Hybridization & Pulldown
Biotin-Streptavidin Probes: GAPDH, Viral Genome
Quantification
B
CHIKV
CHIKV NSP2 Enrichment vs. GAPDH RP (Normalized to Input)
GAPDH
Viral Genome
C
SINV
SINV NSP2 Enrichment vs. GAPDH RP (Normalized to Input)
D
Mock
CHIKV
SINV
GAPDH Enrichment vs. GAPDH RP (Normalized to Input)
E
CHIKV
CHIKV NSP2 Enrichment vs.GAPDH RP (Normalized to Input)
G
GAPDH Enrichment vs.GAPDH RP (Normalized to Input)
F
SINV
SINV NSP2 Enrichment vs. GAPDH RP (Normalized to Input)
H
ALPHA Enrichment vs.GAPDH RP (Normalized to Input)
I
GAPDH
Anti-CHIKV
ALPHA
Ex1/2
Ex2/3
Ex3
Ex1
Ex2
Ex1Truncated
Undiluted
1:10
1:100
1:1000
K
GAPDH
Replicon
nsp1
nsp2
nsp3
nsp4
Undiluted
1:10
1:100
J
500 bp
L
500 bp

Figure S6, Related to Figures 4 and 5: *ALPHA* interacts with CHIKV RNA in cells and *in vitro* (A) *ALPHA*-overexpressing HBMEC were left uninfected or infected with either CHIKV and SINV and crosslinked with glutaraldehyde. Lysates were generated and hybridized with 500mer, biotinylated, antisense, oligonucleotide probes followed by enrichment with streptavidin-conjugated beads. The relative enrichment of (B) CHIKV RNA, (C) SINV RNA, and (D) *GAPDH* were measured by qPCR. (E-H) Wildtype HBMEC were uninfected or infected with CHIKV or SINV and crosslinked with glutaraldehyde. Lysates were generated and hybridized with 500mer, biotinylated, antisense, oligonucleotide probes followed by enrichment with streptavidin-conjugated beads. The relative enrichment of (E) CHIKV RNA, (F) SINV RNA, (G) *GAPDH*, and (H) *ALPHA* were measured by qPCR. (I) Streptavidin dot blot demonstrating the relative biotinylation levels of each RNA used in the *in vitro* RNA interaction assays shown in Figure 5B-D. 200 ng of each RNA was spotted in the top row and diluted as indicated. (J) Agarose gel showing the sizes of each RNA used in the *in vitro* RNA interaction assays shown in Figure 5B-D. 1.5 μg of each RNA was visualized. (K) Streptavidin dot blot demonstrating the relative biotinylation levels of each RNA used in the *in vitro* RNA interaction assays shown in Figure 5E-H. 500 ng of replicon was used. Equal molar ratios relative to the replicon RNA were used for the remaining RNAs and diluted as indicated. (L) Agarose gel showing the sizes of each individual nsp RNA used in the *in vitro* RNA interaction assays shown in Figure 5E-H. 2.5 μg of each RNA was visualized. *p<0.05, **p<0.01, ***p<0.001; error bars are S.E.M.; n=3; Statistical analyses were performed using Student's (unpaired, two-tailed) *t* test (B, C, E, F), one-way ANOVA with Sidak correction for multiple comparisons (D, G, H).

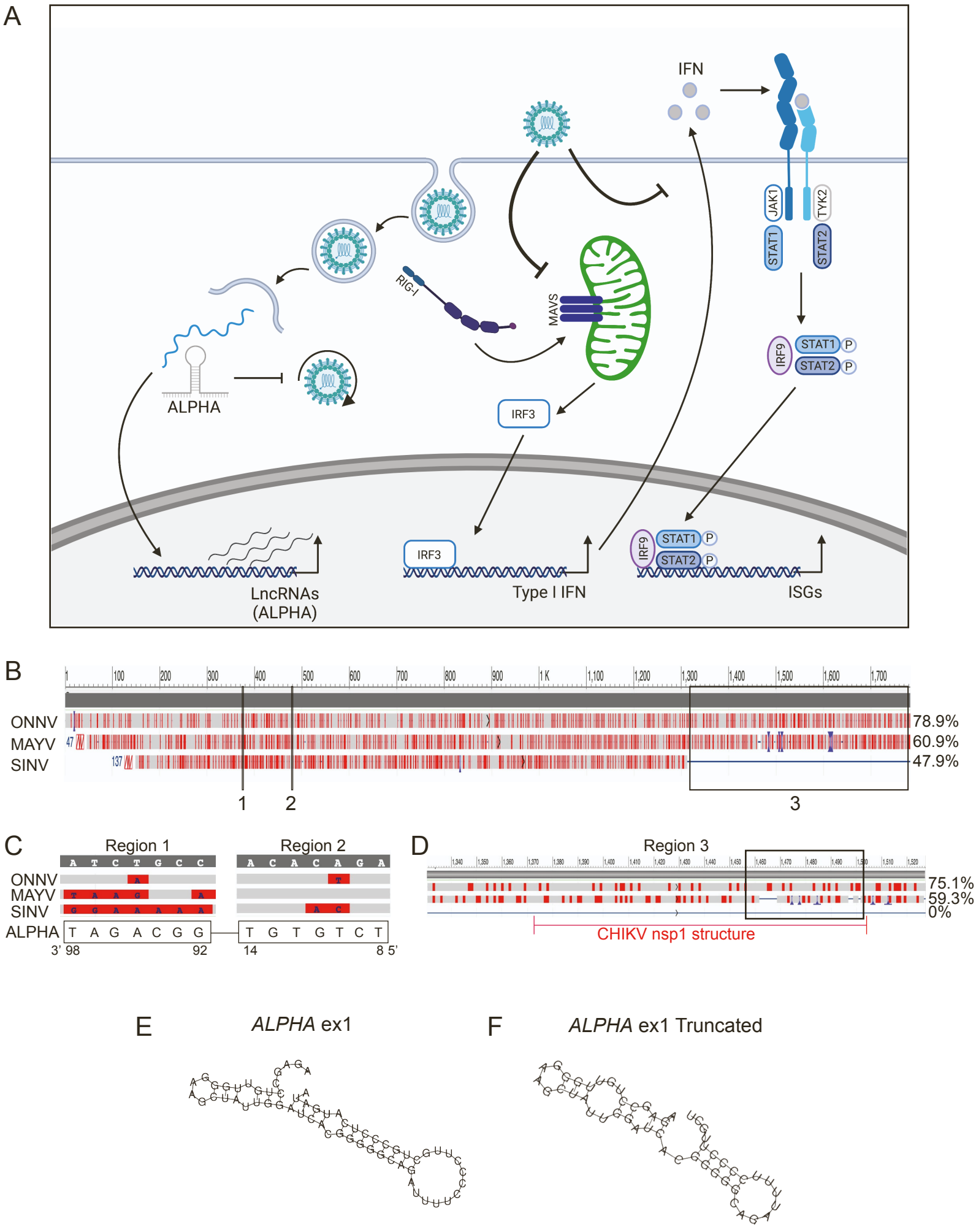
A
IFN
JAK1
TYK2
STAT1
STAT2
RIG-I
MAVS
IRF9
STAT1 P
STAT2 P
ALPHA
IRF3
LncRNAs
(ALPHA)
Type I IFN
ISGs
B
ONNV
MAYV
SINV
78.9%
60.9%
47.9%
1
2
3
C
Region 1
Region 2
ONNV
MAYV
SINV
ALPHA
T A G A C G G
T G T G T C T
3' 98
92
14
8 5'
D
Region 3
75.1%
59.3%
0%
CHIKV nsp1 structure
E
ALPHA ex1
F
ALPHA ex1 Truncated

Figure S7, Related to Figure 5 and Discussion: The functional role of *ALPHA* in innate immunity against CHIKV. (A) Schematic illustrating *ALPHA*'s antiviral function against CHIKV. CHIKV infection results in the activation of classical innate signaling pathways including IFN. However, this response is antagonized by CHIKV. In parallel, many lncRNAs are induced by CHIKV including *ALPHA*, which localizes to the cytoplasm and directly interacts with CHIKV genomic RNA to prohibit viral replication independently of IFN. (B-D) Genomic alignments of the nsp1 gene between related alphaviruses using megaBLAST. (B) Full-length nsp1 is shown with black boxes demarcating putative *ALPHA* binding regions: 1) nucleotides 380-386, 2) nucleotides 484-490, and 3) the 3' end of nsp1. (C) Zoomed in schematics of regions 1 and 2. The complementary sequence withing the *ALPHA* sequence is detailed in the black boxes in the 3' to 5' direction with nucleotide numbers indicated (D) Zoomed in schematic of region 3. The structural element described in Madden, et al. between nucleotides 1377-1506 is demarcated by a red line. Gaps in the MAYV genome are indicated by black lines and highlighted by a black box. (E-F) Secondary structure predications generated using RNAfold for (E) full-length *ALPHA* ex1 and (F) truncated *ALPHA* ex1.